SENSITIVITY AND UNCERTAINTY ANALYSIS OF PLUTONIUM AND CESIUM ISOTOPE RATIOS IN BR3 CORE 4A/B FUEL ROD

A Thesis
Presented to
The Academic Faculty

by

Andrew J. Conant

In Partial Fulfillment
of the Requirements for the Degree
Master's of Science in the
School of Mechanical Engineering

Georgia Institute of Technology
December 2015

SENSITIVITY AND UNCERTAINTY ANALYSIS OF PLUTONIUM AND CESIUM ISOTOPE RATIOS IN BR3 CORE 4A/B FUEL ROD

Approved by:

Dr. Anna Erickson
Committee Chair, Advisor
School of Mechanical Engineering
Georgia Institute of Technology

Dr. Bojan Petrovic
School of Mechanical Engineering
Georgia Institute of Technology

Mr. Martin Robel
Nuclear and Chemical Sciences Division
Lawrence Livermore National Laboratory

Date Approved: 11/23/2015

ACKNOWLEDGEMENTS

TABLE OF CONTENTS

LIST OF TABLES

LIST OF FIGURES

SUMMARY

Characterization of spent fuel from nuclear reactors implements experimental and computational techniques to determine the reactor operating conditions. Furthermore, the analysis relies heavily on computational techniques when knowledge of the spent fuel sample is limited. This research investigated the sensitivity and uncertainty of computationally-predicted ^{240}Pu/^{239}Pu and ^{137}Cs/^{135}Cs isotope ratios to two operating parameters with incomplete information about the operation of the BR3 pressurized water reactor: the location of a fuel rod within an assembly and the boron concentration in the coolant. The computational ratios were compared to experimentally-measured values. The results should provide understanding of how uncertainty in reactor operating parameters impact the isotope ratios. MCNP simulated test cases of the rod location and boron concentration for an assembly-level model of the BR3 core. The results showed a 30% over-prediction of the ^{240}Pu/^{239}Pu ratio compared to the experimental values at the axial center of the rod. The ^{137}Cs/^{135}Cs ratio showed a larger spread but most cases overlapped with the experimental values. In addition, uncertainty quantification using a response function method found systematic uncertainties as high as 36% for the ^{240}Pu/^{239}Pu and 15% for the ^{137}Cs/^{135}Cs ratio due to the rod location. The method found lower uncertainties due to the boron concentration. Disagreement between the experimental and computational values for the plutonium ratio suggests that uncertainty in the reactor operation and the ability to test only a few cases render it difficult to gain information about the operation history of the reactor. Therefore, nuclear forensics faces a significant challenge in acquiring information about nuclear reactor operation from spent fuel samples.

CHAPTER I

INTRODUCTION

Nuclear forensic analysis is defined as the "reliable collection, treatment, analyses, and assessment of evidentiary specimens for elemental, isotopic, chemical, and physical signature species that may provide technical insights into the origins of primary questioned material" [24]. Applications of this analysis include examples important for nuclear security, such as illicit trafficking or smuggling of nuclear material or nuclear terrorism attacks such as improvised nuclear devices (INDs) or radiological dispersal devices (RDDs) [10]. Since 1992, the International Atomic Energy Agency reported more than 2000 instances of illicitly traffickes nuclear material, 400 of which involved natural, depleted, or low-enriched uranium, and 16 instances that contained special nuclear material (SNM) like highly-enriched uranium (HEU) or plutonium [24]. An important consideration for nuclear forensics is the characterization of these intercepted samples that were irradiated in a nuclear reactor.

Isotopic signatures from spent fuel can be used to gain information about the source or history of nuclear material, in particular for spent fuel analysis [17]. The plutonium content in nuclear fuel poses a proliferation concern and is of interest for material control and accountability (MC&A). Characterizing the material from a nuclear reactor can be used for nuclear forensics analysis to conduct attribution, which is especially important when the material origin is unknown [16]. Many different isotopes can be considered for the analysis, yet plutonium and cesium isotopes have been consistently used as forensic signatures [17] [22] [9] [32] as they are produced in relatively high concentrations from the neutron capture on ^{238}U and fission of uranium and plutonium, respectively.

Forensic signatures can be classified into two categories: comparative signatures and predictive signatures. A comparative signature must be analyzed relative to known data, for example within a database of reference samples. Predictive signatures, on the other hand, can be used when no knowledge of similar samples is available. Reactor modeling for nuclear forensic analysis can play a major role in the attribution process via predictive signatures. If a fuel sample is intercepted, it is almost certain that the analysis must be performed without knowledge of the origin of the fuel and the history of the reactor in which it was irradiated. Forensic analysis of predictive signatures can help assess the end use of the reactor operation, whether that be for civilian power or weapons purposes. Many studies have been performed to quantify the isotope inventory to perform fuel performance testing to extend irradiation fuel cycles [23] [18], and now forensic analysis of spent nuclear fuel is becoming more popular in the realm of nonproliferation [4] [19] [26].

In 1984, Idaho National Laboratory (INL) conducted non-destructive and destructive measurements on 100 spent fuel rods in the BR3 core 4A/B reactor [3]. Since 2010, a collaboration between Idaho National Laboratory and Lawrence Livermore National Laboratory (LLNL) was tasked to perform destructive measurements on one of those rods. One of the challenges was the lack of information with regards to the origin of the fuel sample within the core. Documentation of the location and orientation of fuel rods within assemblies could not be obtained. The specifics of the control rod history in the reactor is also not published. This uncertainty provides a unique opportunity to test several operating parameters and to develop a set of benchmarking cases with the experimental values for isotopes of interest.

Experimental analysis of spent fuel samples from BR3 reactor offers an opportunity to conduct an evaluation of the uncertainties in the computationally predicted isotopic composition of the fuel as a function of burnup, neutron poisons, and axial location in the core. The BR3 is an experimental reactor used as a test station for

prototype fuels in realistic PWR conditions. Because of its purpose, the irradiated fuel features enrichments both characteristic of modern PWR fuels and higher (up to 8.26 wt% of ^{235}U.) In addition, the assemblies tested include high burnup (up to 40 GWd/t), burnable poison (Gd) and mixed uranium-plutonium oxide (MOX).

BR3 fuel sample experimental analysis [6] was performed to obtain high-quality radiochemical assay data, and the results were compared against predictive modeling in MCNP. MCNP is routinely used as a modeling and simulation tool for prediction of a fuel rod/assembly/core behavior during irradiation. This comparison of the simulation results with the experimental will also test the ability of a code to predict various parameters for an unusual case: BR3 core 4A/B reactor fuel bundles are short (on the order of 1 meter in active fuel length) with high initial enrichment and a complicated irradiation history.

The simulations were performed to be compared with non-destructive (NDA) and a destructive (DA) analysis of the fuel rods. The NDA was conducted at Idaho National Laboratory and included a gross gamma-scanning of the rod, performed axially to preserve the burnup information. This axial burnup distribution was replicated in the simulation. The second step is the DA of the rod involving actinide content measurement and important fission product identification [3].

Modeling and simulation of BR3 core 4A/B were complicated by the lack of knowledge of the exact rod location within assembly or core. Moreover, little information was available on the overall core composition and reactivity control history, two parameters that have an impact on the neutron flux spectrum in the reactor and, in turn, isotope concentrations in its fuel rods. Intercepted fuel materials would often be associated with a lack of knowledge, and sufficient data to which experimental isotopic signatures can be compared does not exist today [4].

1.1 Objective

The objective of this research is to analyze the effect of systematic uncertainty in reactor operating parameters on isotope ratios of an irradiated fuel rod. The two reactor operating parameters of interest for this fuel rod are its position in the assembly and boron concentration in the coolant. The two isotope ratios of interest are ^{240}Pu/^{239}Pu and ^{137}Cs/^{135}Cs. The predicted isotope ratios were compared to experimental values.

A novel method was constructed to calculate the effect of systematic uncertainty on the isotope ratios. A response function quantified the change in isotope inventory based on changes in reactor operating parameters. This response function was formulated as the basis for the propagation of systematic uncertainty.

It is important to note that although the results were compared to the experimental data and an uncertainty analysis was performed, a firm conclusion in the location of the rod cannot be made. The BR3 reactor has many uncertainties in its operation, therefore discovering the location of the rod during 4A/B operation within reasonable uncertainty is nearly impossible.

CHAPTER II

TECHNICAL BACKGROUND

2.1 Spectrometry

The experimental data for this project is given from measurements perfomed by Idaho National Laboratory (INL) and Lawrence Livermore National Laboratory (LLNL). The first of these measurements took place by INL in 1984 [3]. Measurements on rod I-316 (the rod of interest) and other rods were taken, including a neutron radiograph and gamma scans. Gross and isotopic gamma scans, which outline the shape of axial burnup, of the rod are shown in Figure 1. Peak rod average powers were also given for the rod over a two-month period of reactor operation. The rod average burnup was listed as 39.4 GWd/tHM, although the report does not discuss the method for determining this value. The gamma scans and rod average burnup provide enough information on the shape and magnitude of the expected burnup.
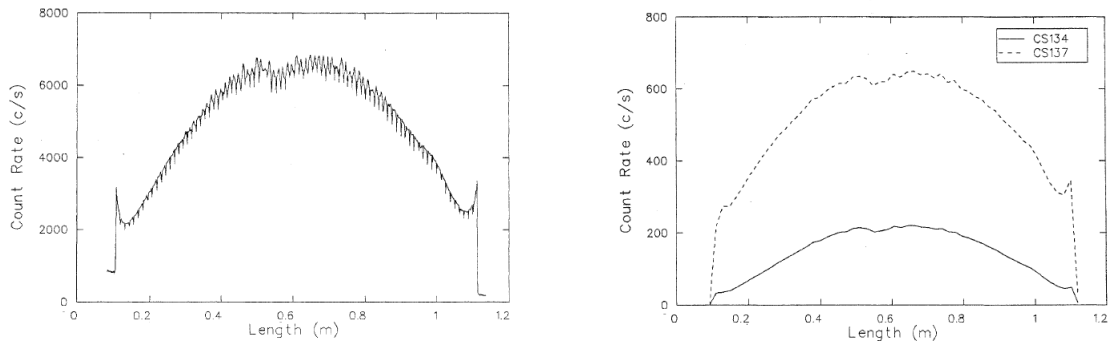
Figure 1: Gross (left) and isotopic (right) gamma scan for rod I-316, reproduced from [3]

In 2013, LLNL performed more measurements on rod I-316. Measurements of plutonium and cesium isotope ratios at eight different axial locations in the rod of interest were performed using chemical separation followed by either quadropole or

multi-collector inductively-coupled plasma mass spectrometry (ICP-MS) [24]. The plutonium and cesium isotope ratios of interest for this study, ^{240}Pu/^{239}Pu and ^{137}Cs/^{135}Cs, with their reported uncertainties to 2σ are shown in Table 1. These are the experimental ratios to which the modeled results were compared.

Table 1: Plutonium and cesium isotope ratios from I-316 fuel rod sampling, obtained from [28]

Axial Position (cm)	^{240}Pu/^{239}Pu	$\pm 2\sigma$	^{137}Cs/^{135}Cs	$\pm 2\sigma$
0.0 (bottom)	0.2453	0.0032	1.04	0.05
14.9	0.2544	0.0030	1.05	0.06
28.5	0.3258	0.0042	1.23	0.07
43.4	0.3620	0.0046	1.32	0.06
57.4	0.3580	0.0047	1.28	0.07
72.1	0.3235	0.0043	1.19	0.05
86.9	0.2165	0.0029	0.89	0.05
100.5 (top)	0.2123	0.0029	0.92	0.05

2.2   BR3 Reactor

The BR3 reactor was a Belgian experimental pressurized water reactor (PWR) which served as a prototype reactor for commercial-size plants. It was operated by the Belgian Nuclear Research Center SCK-CEN and was used to test nuclear fuels and neutron physics [1]. The BR3 operated from 1962 to 1987, and went through a total of four core and fuel modifications, including operation as a spectral shift reactor known as the Vulcain project [30]. The last operational core of the BR3 reactor was composed of oxide fuel (including mixed-oxide fuel) and moderated by light water. It was shut down in 1987, and the reactor went into decommissioning, which was chosen as the pilot project for the decommissioning of PWRs in Europe [8]. Since the decommission began, the spent fuel was stored on site in the deactivation pool as well as distributed to various laboratories in Belgium and abroad.

This analysis is focused on the fourth-type core (BR3/4) of the reactor, which was in operation between 1976 and 1987. Specifically, the assemblies of interest included

6
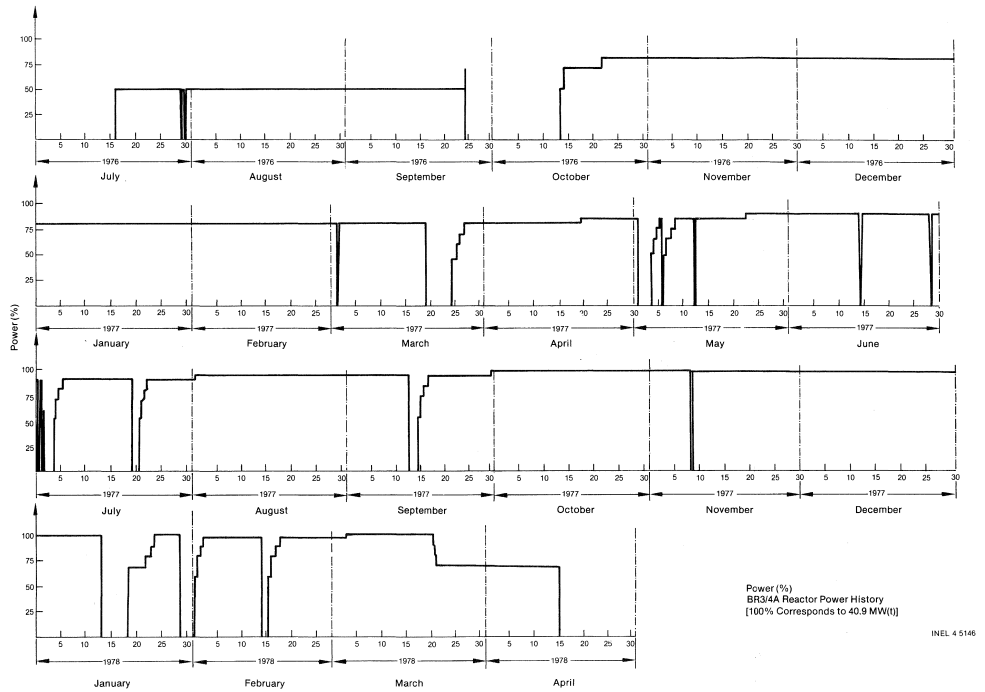
Figure 3. BR3/4A reactor power history.

Figure 2: Full power history for cycle 4A, reproduced from [3]

samples that were irradiated in both the BR3 4A and BR3 4B cycles. Both 4A and 4B cycles have a rather complicated power history since the reactor was used extensively for physics testing and operator training. Their actual power histories are shown in Figures 2 and 3 [3]. This power history contains many changes in power level and numerous (over seventy) shutdowns.

The BR3 reactor core 4A/B was composed of 73 hexagonal fuel assemblies of four general types: 'g'-type, 'G'-type, 'go'-type, and 'Z'-type. Experimental samples were obtained from batches of rods from series 300, corresponding to 'go'-type assembly as shown in Figure 4. A map of the core of 4A is shown in Figure 5. Rod I-316 came from one of the 'go'-type assemblies, and more specifically, one of the 'go*' assemblies in Figure 5. It can be seen that all of 'go*' assemblies are surrounded by four fuel assemblies and two water channels.

7
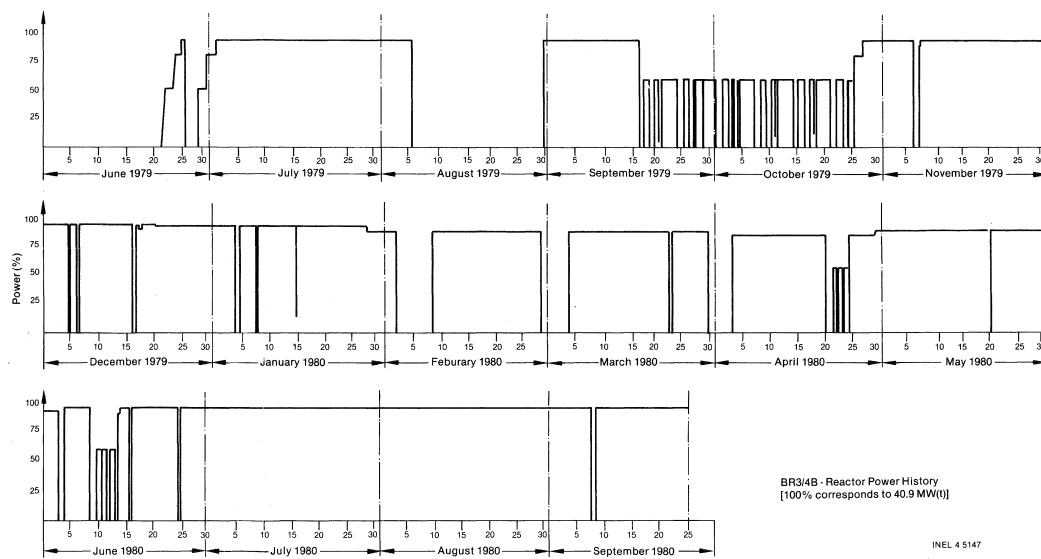
Figure 5.   BR3/4B reactor power history.

BR3/4B - Reactor Power History
[100% corresponds to 40.9 MW(t)]

INEL 4 5147

16

Figure 3: Full power history for cycle 4B, reproduced from [3]

8

Prior to irradiation in core 4A, the fuel rod of interest (referred to as the ROI) was located in a 'go'-type assembly composed of twelve uranium rods, twelve MOX rods, and four uranium-gadolinium rods (assembly type labeled as 'go-12-4'). The isotopic composition of each type of those rods is shown in Table 2. The location of the ROI in the assembly and the assembly to which it belongs are not available in the literature.

Table 2: Isotope composition by weight of three types of rods in 'go-12-4' assembly

Rod Type	Isotope	Weight %
UO_2	^{235}U	7.280
	^{238}U	80.860
	^{16}O	11.860
MOX	^{235}U	0.511
	^{238}U	80.592
	^{239}Pu	4.744
	^{240}Pu	1.644
	^{241}Pu	0.472
	^{242}Pu	0.193
	^{16}O	11.845
U-Gd	^{235}U	4.760
	^{238}U	74.569
	^{16}O	11.995
	^{155}Gd	1.284
	^{156}Gd	1.776
	^{157}Gd	1.358
	^{158}Gd	2.155
	^{160}Gd	2.103

All of the 'go-12-4' assemblies are located in the mid-region of the core. It can be assumed that the all of the assemblies of 'go'-type experienced similar levels of flux as they were at the same radial distances from the center of the core. However, the proximity of the ROI to surrounding assemblies and water channels (or control rods) will have an impact on the local neutron flux to which it is subjected.

Is is difficult to determine what the most likely configuration of the rods in the assembly could have been. No literature on the exact location of the rods is known. However, Yamamoto et al. [35] showed the rod configuration for a 'go'-type assembly

from another core of the BR3, which places the MOX rods towards the center and only a few UO_2 rods on the periphery. It is unclear if the assembly of interest for the BR3 4A/B core had a similar configuration.

Table 3: Description of BR3 fuel assembly types

Assembly Type	Number in Core	Rods per Assembly	Rod Pitch	^{235}U wt%	Fissile Pu wt%
go	40	28	Square 1.35 cm	5.76% 8.26%	9%
g	6	28	Square 1.26 cm	6.2% 6.4% 8.6%	none
G	19	20	Square 1.41 cm	from 3.0% to 8.6%	3.8% 7.0%
Z	8	36	Hexagonal 1.41 cm	3.0% 7.1%	5.0%

The reactivity of the core was controlled with soluble boron in the coolant and tubular control rods [6]. The boron concentration history for the 4A core is shown in Figure 6. The boron concentration history for core 4B is not available. Limited information is known about the control rod operation. Storrer [30] discusses the use of control rods for the BR3 Vulcain project, which involved using a mix of H_2O and D_2O as the moderator coolant, known as a spectral shift reactor. He states that the tubular control rods are composed of a 2% boron stainless steel and provides the
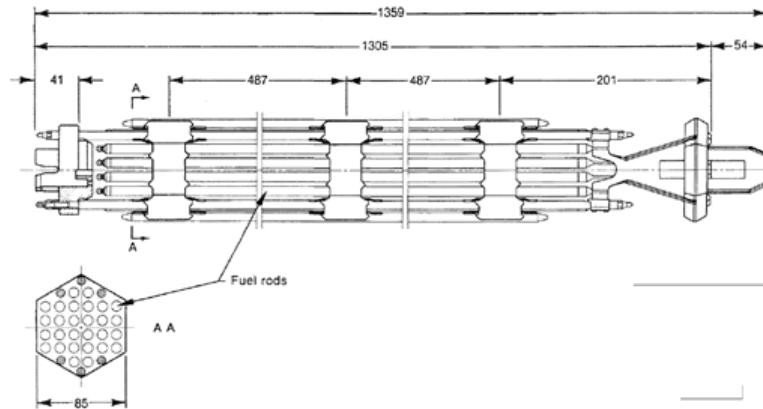
Figure 4: BR3 fuel assembly of 'go'-type, dimensions in mm, reproduced from [3]
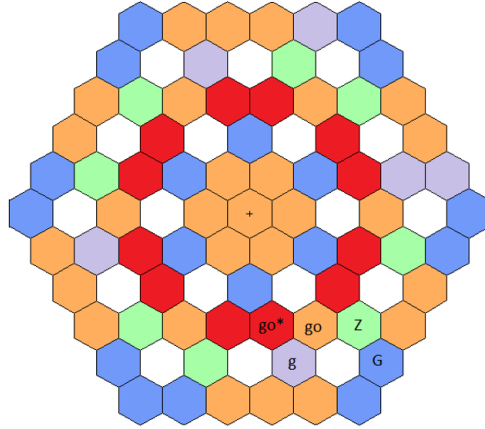
Figure 5: BR3 4A core map noting the four different assembly types. One of the 'go*'-type assemblies contains the ROI. White designates water channels. (detailed in Table 3)

inner and outer radius of the control rods. A conclusion cannot be made about the control rods for 4A/B compared to the Vulcain project as including heavy water in the moderator will have an impact on the flux spectrum.
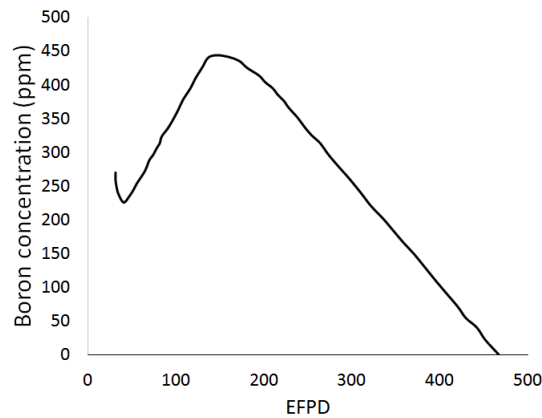
Figure 6: BR3 boron concentration curve for cycle 4A, reproduced from [6]
.

2.3 Isotopes of Interest

The four main isotopes of interest for this project are ^{239}Pu, ^{240}Pu, ^{135}Cs, and ^{137}Cs. Their main production and destruction mechanisms inside a reactor will be described here.

11

^{239}Pu is a fissile plutonium isotope that is not naturally-occurring. The main production mechanism in a nuclear reactor is due to the capture of a neutron on ^{238}U, which is most common in the fast energy range. The main destruction mechanism is due to its capture (either fission or absorption) of a thermal neutron. It has a half-life of approximately 24,000 years.

$$^{238}_{92}U + ^{1}_{0}n \rightarrow ^{239}_{92}U^{*} \xrightarrow{23.5mins} ^{239}_{93}Np \xrightarrow{2.36days} ^{239}_{94}Pu$$
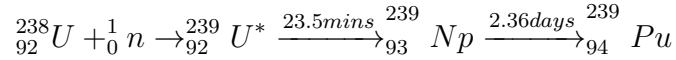
^{240}Pu is a fissionable isotope of plutonium that is not naturally-occuring. The main production method is through the capture of a neutron on ^{239}Pu. The main destruction method is due to its absorption of a neutron: it has a large resonance on the order of eV (see Figure 7). It has a half-life of approximately 6,500 years.

$$^{239}_{94}Pu + ^{1}_{0}n \rightarrow ^{240}_{94}Pu$$
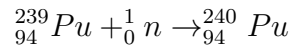
^{135}Cs is a direct fission product and produced through the decay of short-lived fission products. The main production mechanism in a reactor is the decay of ^{135}Xe, which has a thermal fission yield of 6.61% for ^{235}U and 6.33% for ^{239}Pu (according to ENDF [5]). ^{135}Xe, produced from the decay of short-lived ^{135}I, has a large thermal neutron resonance absorption of approximately 2 Mb. ^{135}Xe, therefore, has a significant mechanism that competes with its decay to ^{135}Cs. The production of ^{135}Cs is largely dependent on the flux, which impacts the absorption rate of ^{135}Xe. ^{135}Xe has a half-life of 9.1 hours. There are not any significant destruction mechanism of ^{135}Cs in nuclear reactors as its cross-section is low and its half-life is around 2.3 million years.

$$^{135}_{54}Xe \xrightarrow{9.14hrs} ^{135}_{55}Cs$$
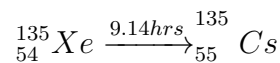
^{137}Cs is a fission product, with a relatively small instantaneous fission yield for both ^{235}U and ^{239}Pu. It does however, result from the decay of precursors ^{137}I and

^{137}Xe. Its cumulative fission yield is mainly due to the decay of these isotopes. The yields for for ^{235}U and ^{239}Pu are 6.221% and 6.588%, respectively [25]. These yields show that the fission yield changes around 5% if all the fissions in a reactor went from all ^{235}U Its main destruction mechanism is its decay. It has a half-life of 30.2 years.

$$^{137}_{55}Cs \xrightarrow{30.2yrs} {}^{137m}_{56}Ba$$
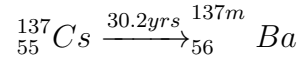
Several important factors that apply to this project must be noted here. The thermal neutron flux has a significant impact on the amount of ^{239}Pu (due to thermal fission) and ^{135}Cs (due to competing capture mechanism of ^{135}Xe). The epithermal neutron flux has a significant impact on the amount of ^{240}Pu due to its resonance. Both ^{239}Pu and ^{240}Pu are directly affected by the fast flux as they are produced due to neutron capture of ^{238}U. ^{137}Cs is the only one of these isotopes with a half-life for consideration in the analysis of spent fuel. All of the relevant cross-sections for the reactions discussed above, as well as the cross-section for ^{10}B, are shown in Figure 7.
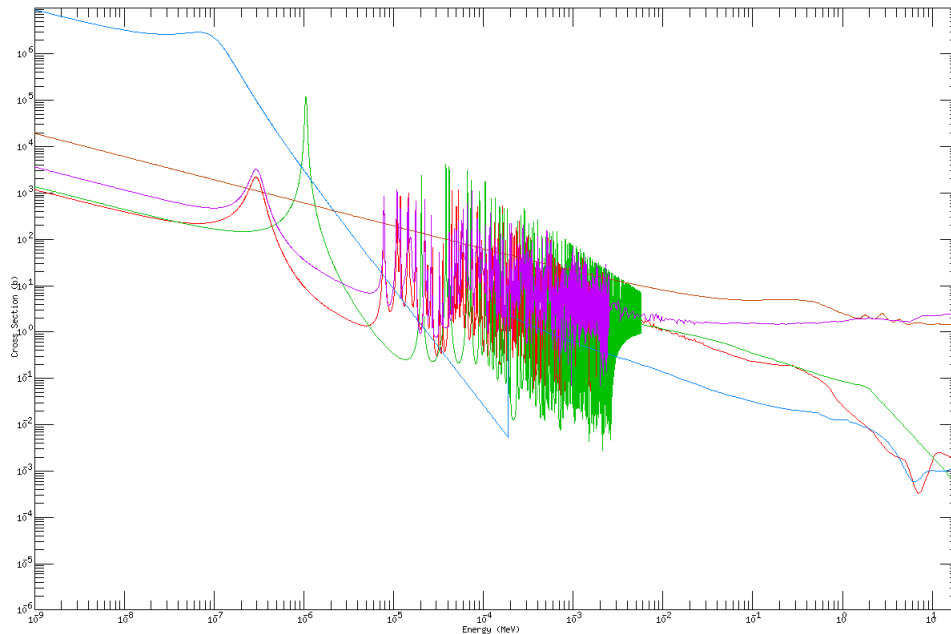
Figure 7: Cross-sections for isotopes relevant for the study of plutonium and cesium isotopes: ^{239}Pu capture (purple), ^{239}Pu fission (red), ^{240}Pu capture (green), ^{135}Xe capture (blue), ^{10}B reaction (brown), taken from ENDF [5]

13

2.4   MCNP6 and Uncertainty

The Monte Carlo N-Particle transport code system was the code used to conduct the sensitivity and uncertainty analysis. It is a "general purpose, continuous energy, generalized geometry, time dependent Monte Carlo code" for radiation transport [2]. The version of MCNP being used is 6.1 which has major improvements in run speed and memory allocation (particularly for parallel jobs) as compared to MCNP5 and MCNPX [14][11]. MCNP was chosen as the code system to be used as it is commonly used for criticality and depletion (time-dependent) calculations.

MCNP6 maintains the ability to model general geometries with many capabilities for criticality/burnup calculations (outlined in the MCNP6 manual [2]), which will be described in this paragraph. The KCODE card calculates the multiplication factor, k_{eff}, with a user-specified number of source particles per generation, initial guess for the multiplication factor, inactive cycles, and active cycles. The source neutrons in each cycle follow the Watt fission spectrum and are equally spread through the locations specified by the KSRC card. MCNP6 can be used in a time-independent manner for shielding or criticality calculations but can also be time-dependent with implementation of the BURN card for depletion calculations. The BURN card links MCNP6 to CINDER90 [34], which implements 63-group cross-section data. When an MCNP6 input contains the BURN card, the code performs the KCODE calculation twice, once at the beginning of the time step and another at the end of the time step, following predicted isotope depletion from the first estimate of the flux and eigenvalue. The final estimate for the flux and eigenvalue are taken as the average of the beginning and end of cycle estimates.

MCNP also possesses the ability to calculate cell fluxes with user-specified energy bins [2]. It does so by using a track-length estimator, i.e. how far the average neutron neutron travels in that cell. The F4 tally, for example, calculates the flux by dividing the length the neutron travels in a cell divided by that cell's volume [29].

Tally multiplier cards can also be used to calculate reaction rates. MCNP can be instructed to do this by simply multiplying by the cross-section of the material that fills the cell by the tally-determined cell flux.

As a Monte Carlo code, MCNP6 is a stochastic code. Its predictions must be examined with respect to statistical uncertainty, which forever persists in MCNP as only a finite number of particles can be simulated [12]. Unfortunately, MCNP6 solely reports statistical uncertainties for the eigenvalue and tallies. It does not report uncertainties for predicted isotopes, the object of this study. MCNP6 systematic uncertainty involves the precision of cross-sections used in the calculations as well as other input parameters, such as the reactor power, temperatures, etc. The nuclear community has devoted significant effort into quantifying the uncertainty associated with the cross-sections [13][31]. This research examined the uncertainty associated with reactor operating parameters, which are other parameters besides the cross-section data that are inputs in the MCNP code.

CHAPTER III

METHODOLOGY

3.1   Modeling

A portion of the BR3 core was modeled in the Monte Carlo N-Particle (MCNP6) transport code system [2]. The portion of the core that is modeled is a seven-section model, which consists of the assembly of interest, two water channels (where control rods would have been inserted), and four other assemblies. The rod of interest is located in the central assembly, which is a 'go'-type assembly with 12 UO_2 rods, 12 MOX rods, and 4 U-Gd rods. These surrounding assemblies are modeled to be the same as the central 'go'-type assembly (without the rod of interest) due to the unavailability of surrounding assembly information. The active fuel length of 100 cm is split up into 50 axial cells of 2 cm each, which is small enough for good axial resolution of the ratios but not too small such that the length is smaller than the distance associated with physical processes in a nuclear reactor [12]. The length of moderator above and below the axial ends of the moderator is set to 5 cm to save computation time; a discussion of the implications of this value on the flux is present later in the results section.

The fuel, cladding, and coolant temperatures are all calculated using a single-channel analysis, as described by Todreas & Kazimi [33]. The inlet and outlet coolant temperatures are assumed to be 255 °C and 270 °C, which are values cited for core 4D of the BR3 [27]. The axial distribution of those temperatures are shown in Figure 9. The coolant density profile is shown in Figure 10.

The actual power history (see Figures 2-3) detailed many shutdowns and changes in power. A change in power requires at least another time step in the MCNP6

BURN card, therefore modeling the detailed power history would be computationally expensive. The BR3 power history can be divided into a reasonable amount of time steps for reactor modeling; specifically 38 time steps are used. This simplified power history is shown in Figure 8, where the split between core 4A and 4B is at the 433 day shutdown. Small time steps must be used near the beginning of each startup from zero power to include the transient effects to xenon equilibrium. The number of steps within each step at full power ranged from 3 for the 45 days at 88% power to 7 for the 522 days at 88% power.

The cases described below are run on the Livermore Computing (LC) Center cluster machines. The LC computer clusters possess the ability to perform sizable and parallelizable jobs. Access to these resources permitted the use of a large number of runs. These machines had access to MCNP6 and most of the sufficient cross-section libraries for this project.

The cross-section libraries that were used for this project are the ENDF/B-VII.0 cross-sections at the relevant temperatures. This corresponded to the .71c, .72c, and .73c libraries in MCNP at the appropriate temperatures [7]. Little changes were made between ENDF/B-VII.0 and ENDF/B-VII.1 for most of the important cross-sections used for this project [5]. The $S(\alpha,\beta)$ cards include additional physics that describes thermal neutron scattering with molecular compounds at low energies, therefore they were also implemented in the models [2].

The full reactor power (40.9 MWt) is known, yet information on the power fraction of each assembly is not available. This means that the power of the model is unknown. However, the average burnup of the rod of interest is known. The BURN card in MCNP, however, only allows the user to input the power and check the burnup once the simulation is completed. It does not allow for the model to be run until a certain burnup. One cannot calculate the burnup of the ROI directly as each power level of the model results in a corresponding flux distribution of the entire assembly model.

17
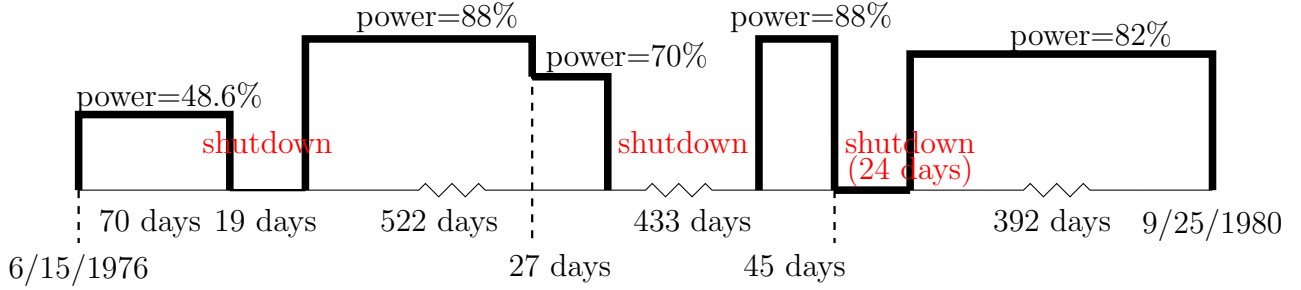
Figure 8: Simplified BR3 4A/B reactor power history with a full power of 40.9 MWt

Because the experimental burnup is known, the assembly power was varied in the simulation in an iterative approach to match the burnup. For example, the model was first run at a certain fraction of the total core power. Given whether the predicted burnup was higher or lower than the experimental burnup, the power of the model was either decreased or increased, respectively. This process was repeated until the predicted burnup is within 2% of the experimentally measured burnup (39.4 GWd/tHM), as it was difficult to match the burnup exactly.

All rods of the same type (other than the rod of interest) are grouped into the same material for each 2 cm axial slice. In other words, all MOX rods of the , for example, are tracked and depleted as the same material. This is a major simplification used to decrease run time, as it is memory intensive to track a lot of materials in MCNP. This reduces the number of materials to be tracked from approximately 4400 to 200.

3.1.1 Sensitivity Analysis

Selecting cases of the ROI position within its assembly was done to test the sensitivity of the isotope ratios. The cases were selected under the assumptions that 1) the rod arrangement in the assembly followed quarter-symmetry, and 2) the rod placement was justified from a general neutronics perspective (for example, the burnable absorber U-Gd rods would not be placed on the periphery of the assembly as the power need not be suppressed there).

Four test cases of the ROI position within the assembly were created using the
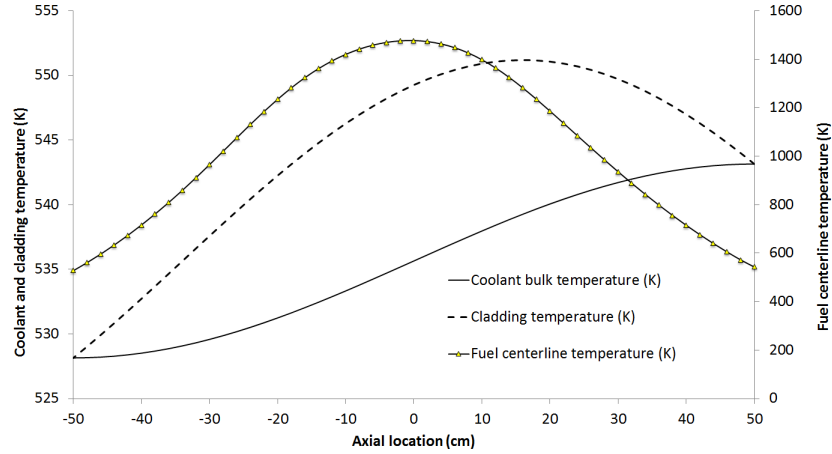
Figure 9: Axial temperature distributions of the fuel, cladding, and moderator as calculated from the single-channel analysis (Note: -50 cm represents the bottom of the rod)
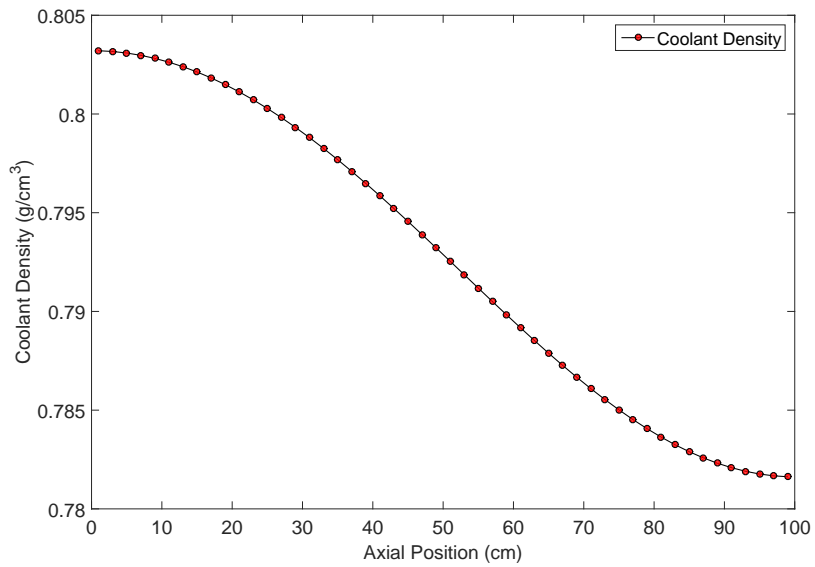
Figure 10: Coolant density as calculated from the single-channel analysis (Note: 0 cm represents the bottom of the rod)

assumptions above. First, the U-Gd rods are placed neither at the center nor periphery of the core. If the U-Gd rods were all placed near the center in a symmetric fashion, a flux suppression would exist at the center of the assembly. Similarly, the U-Gd were not placed at the periphery as the flux does not need to be suppressed there. The U-Gd rods for all four cases are thus placed in the same location at the

mid-region radially in the assembly. The configuration of UO_2 and MOX rods within a similar assembly from Yamamoto et al. [35] generally placed the MOX rods near the center of the assembly and the UO_2 rods at the periphery. It is unclear if the assembly of interest for the BR3 4A/B core had a similar configuration, yet it would make sense to have the UO_2 rods at the periphery and the MOX rods towards the center as the UO_2 rods have a higher fissile loading content (8.26% ^{235}U in the UO_2 rods compared to 4.7% ^{239}Pu with 0.5% ^{235}U in the MOX rods). Therefore, cases one and two were created with this configuration, where case one has the ROI closer to the adjacent assembly, and case two has the ROI closer to the water channel. These placements of the ROI were chosen to examine the impact of the water channel on its isotope inventory at discharge. Some core arrangements, however, tend to place MOX assemblies near the periphery of the core [15], therefore it is possible that the MOX rods in this assembly were placed at the periphery. Cases three and four then had the UO_2 and MOX rods swapped from cases one and two; the MOX rods were on the periphery and the UO_2 rods are near the center. Similar to cases one and two, case three placed the ROI closer to the surrounding fuel assembly and case four placed it closer to the water channel. The axial cross-sections of the four cases are shown in Figure 11.

Selecting cases of the boron concentration were tested with knowledge of the boron concentration history in the coolant for core 4A (see back to Figure 6). The four compositions of boron in the coolant are 100, 200, 300, and 400 ppm of natural boron. These concentrations fall within the 0-450 ppm range from core 4A. The boron concentration in the coolant is held constant throughout the simulation. The ROI position is the same as it was for case one above (see Figure 11).
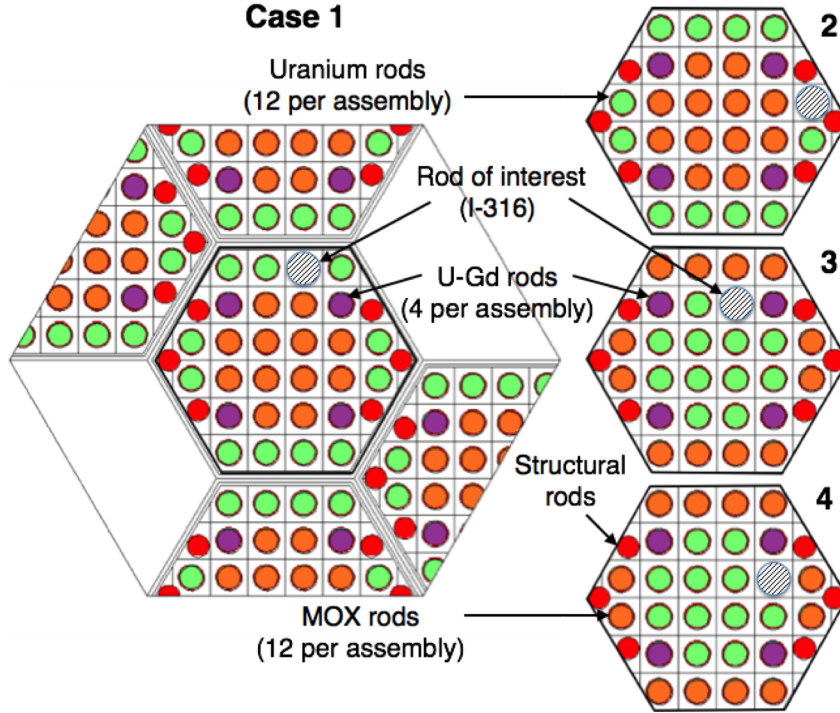
Figure 11: Assembly map of the four cases of the position of the rod of interest

3.2   Uncertainty Analysis

The error of the predicted isotope ratios were calculated based on the uncertainty in the rod position and boron concentration. The boron concentration is a core-wide constant value; it was assumed to be uniformly distributed in the coolant. Therefore a simple response function for the effect of the boron concentration on the ratios was created. The rod position, however, is a difficult parameter to quantify; a rod's discharge isotope inventory is a function of the fissile material, poisons, and moderating material in a volume surrounding the rod. The uncertainty on the isotope concentrations in the rod of interest can be approximated from the response function with respect to these rod parameters. The methodology to propagate the uncertainty of rod position is described below.

A set of response functions for isotope concentrations $(I_1 \ldots I_m)$ that are approximated as linear combinations of rod position variables $(x_1 \ldots x_n)$ can each be expressed as follows:

$$I_k = \sum_{i=1}^{n} A_{ki} x_i = A_{11} x_1 + A_{12} x_2 + ... + A_{in} x_n$$

Here, each A_{kn} is a coefficient associated with an isotope concentration I_k and position variable x_n. The way in which this position variable was quantified is discussed in the results section. Let I_k represent the isotopic inventory in spent reactor fuel for the kth configuration of rod layout in the assembly of interest. The variance-covariance matrix on the isotope concentration of a vector of these isotopes $\vec{I}$ is then:

$$\Sigma^I = A \Sigma^x A^T$$

For n variables, $\mathbf{A}$ is a matrix of coefficients:

$$
\mathbf{A} =
\begin{bmatrix}
A_{11} & A_{12} & ... & A_{1n} \\
A_{21} & A_{22} & & \\
\vdots & & \ddots & \\
A_{n1} & & & A_{nn}
\end{bmatrix}
$$

and Σ^I is a square variance-covariance matrix of the form:

$$
\mathbf{\Sigma}^x =
\begin{bmatrix}
\sigma_1^2 & \sigma_{12} & ... & \sigma_{1n} \\
\sigma_{21} & \sigma_2^2 & & \\
\vdots & & \ddots & \\
\sigma_{n1} & & & \sigma_n^2
\end{bmatrix}
$$

For a single isotope I_k, this equation reduces to its scalar form:

$$\sigma_I^2 = \sum_{i=1}^{n} a_i^2 \sigma_i^2 + \sum_{i}^{n} \sum_{j \neq i}^{n} a_i a_j \rho_{ij} \sigma_i \sigma_j$$

where a_i is a coefficient for the ith variable and σ_i is the uncertainty of the ith variable and ρ_{ij} is the correlation coefficient between variables x_i and x_j.

CHAPTER IV

RESULTS

4.1 Sensitivity Analysis

The four test cases used the iterative method described above to match the burnup to the experimental. Each case took approximately 3-4 iterations to fall within the following burnups. A tolerance of 2% of the experimental burnup was applied. Therefore, the simulation for each case where the average burnup fell within the tolerance operated under a different power. The model powers and final burnups of the four cases are shown in Table 4.

The parameters used for KCODE were 100,000 source particles with 50 skipped cycles and 200 active cycles. The run times are listed in Table 5. These run times reported in computing hours resulted in approximately two weeks of time on computer clusters, including both run and queue time. Note that the run times differ by a noticeable amount due to changes in node and process numbers on the Livermore Computing (LC) machines for the runs. The number of nodes was changed throughout in an effort to examine the optimal number to use. The combination described above satisfied practical limits for run times under the iterative burnup matching method described previously. The statistical errors for the eigenvalue (k_{eff}) were 13-15 pcm for all time steps, and the flux errors were less than 5% for non-trivial energy groups.

4.1.1 Rod Position

The ^{240}Pu/^{239}Pu ratios for the different ROI position cases are shown in Figure 12. The plutonium ratio follows the general axial cosine shape associated with the axial flux. It can be seen that the predicted ratio was considerably higher than the

Table 4: Comparison of experimental, taken from [3], and MCNP-predicted axial average burnups

Case	Model Power (MW)	Rod Average Burnup (GWd/tHM)	Percent Difference from Experimental
Experimental		39.4	
1	1.7201	39.35	-0.12%
2	1.2206	40.10	1.77%
3	1.9450	38.75	-1.65%
4	1.7494	39.47	0.13%

Table 5: Run times for cases of rod position

Case	Run time (computing hours)
1	3998
2	3708
3	4147
4	4171

experimentally measured ratio, particularly near the center. The exact reason for this is unknown.

The MCNP-predicted ^{240}Pu/^{239}Pu ratio and burnup (which have been postulated to have a linear relationship with burnup [20] [21] [24]) as a function of axial position were normalized to their average to examine whether the shape was consistent with the experimental. Figure 13 showed that the shapes are consistent; this meant that the magnitude of the assembly-level prediction for plutonium was high.

The ^{137}Cs/^{135}Cs ratios for the different ROI position cases are shown in Figure 14. The predicted ratio for case two was much higher than that of the experimental and other cases. The other three cases predicted the ratio to roughly fall within the experimental data uncertainties. Case three appeared to fall the most inline with the experimental data.

The over-prediction of the cesium ratio for case two was explained by Figure 15, which showed a 5% over-prediction for ^{137}Cs and 10% under-prediction for ^{135}Cs relative to the next closest case. This resulted in a ^{137}Cs/^{135}Cs ratio much higher
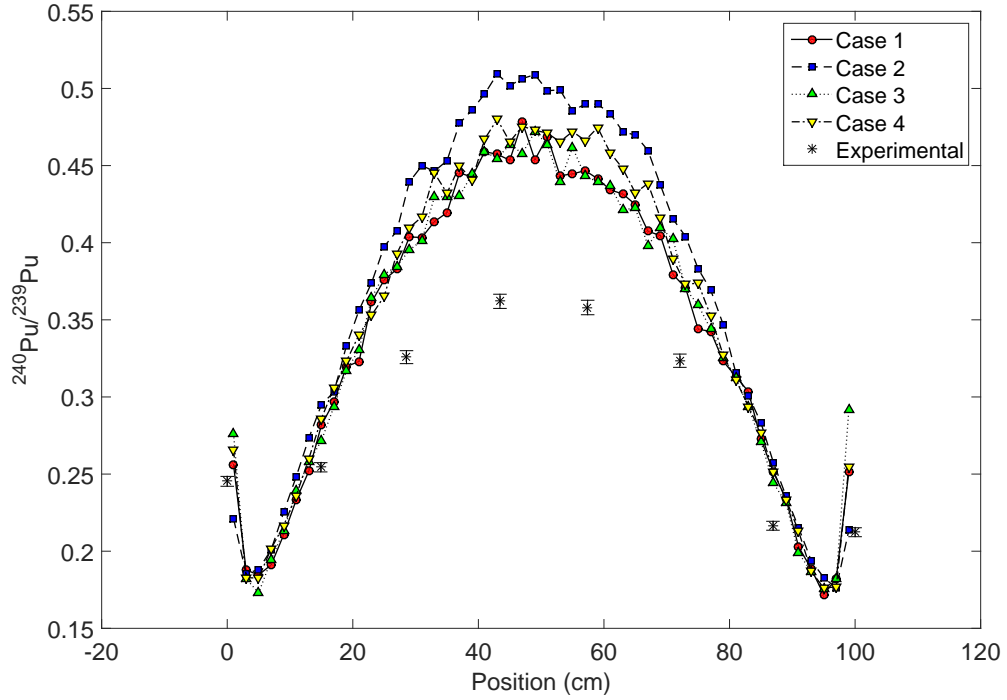
Figure 12: ^{240}Pu/^{239}Pu ratio for the four cases of ROI position

than the other three cases. The ^{135}Cs concentration was lower due to the higher thermal flux there, increasing the capture on ^{135}Xe, the competing mechanism for ^{135}Cs production. The ^{137}Cs was 5% higher because the ROI had a higher power in that pin compared to the ROI in the other rod position cases.

The neutron flux spectrum at the beginning of cycle 4A and end of cycle 4B are shown in Figure 16. The flux spectrum for cases one and two, where the rod of interest was at the periphery of the assembly, were significantly higher than that of cases three and four. Despite the higher flux for cases one and two throughout each time step, the ROI still predicted the same burnup as cases three and four. The average errors of the flux tallies were below 5% for all relevant energy groups for all cases and are shown in Figure 17, which revealed that the flux was well converged.

It can be seen that the ^{240}Pu/^{239}Pu ratio appears more statistically noisy compared to ^{137}Cs/^{135}Cs. This behavior can be explained by the MCNP calculation
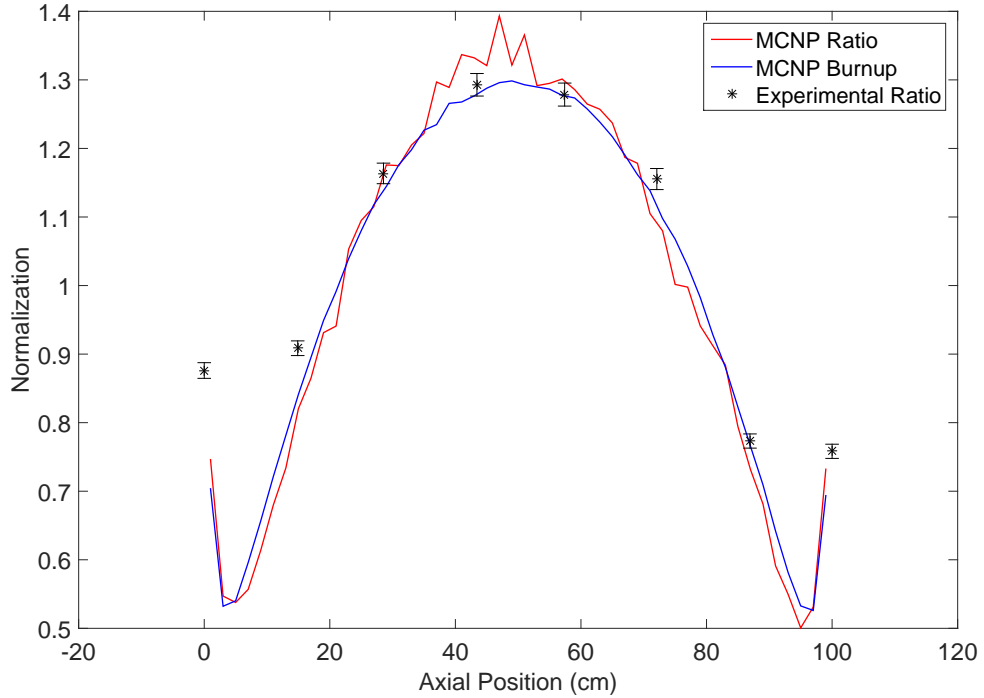
Figure 13: Normalization to the average of MCNP-predicted (case 1) and experimental values

method. The cesium isotopes are dependent on the number of fissions. The ^{137}Cs concentration, in particular, is produced as just a certain fraction of fissions. ^{135}Cs is similar except that it is more sensitive to the flux spectrum due to the ^{135}Xe capture. The plutonium isotopes, on the other hand, are not produced until there is a capture on ^{238}U, which is independent of the number of fissions. Further, the ^{240}Pu convergence is dependent on the convergence of ^{239}Pu. The ratio of ^{235}U and ^{239}Pu fission to ^{238}U capture was between 3-6 for all time steps of all cases; this confirms the worse statistics in plutonium compared to cesium.

4.1.2 Boron Concentration

The ^{240}Pu/^{239}Pu ratios for the different cases of coolant boron concentration are shown in Figure 18. Again, these plots showed an over-prediction of the ratio for all the cases compared to the experimental data. The ratio for all cases tended
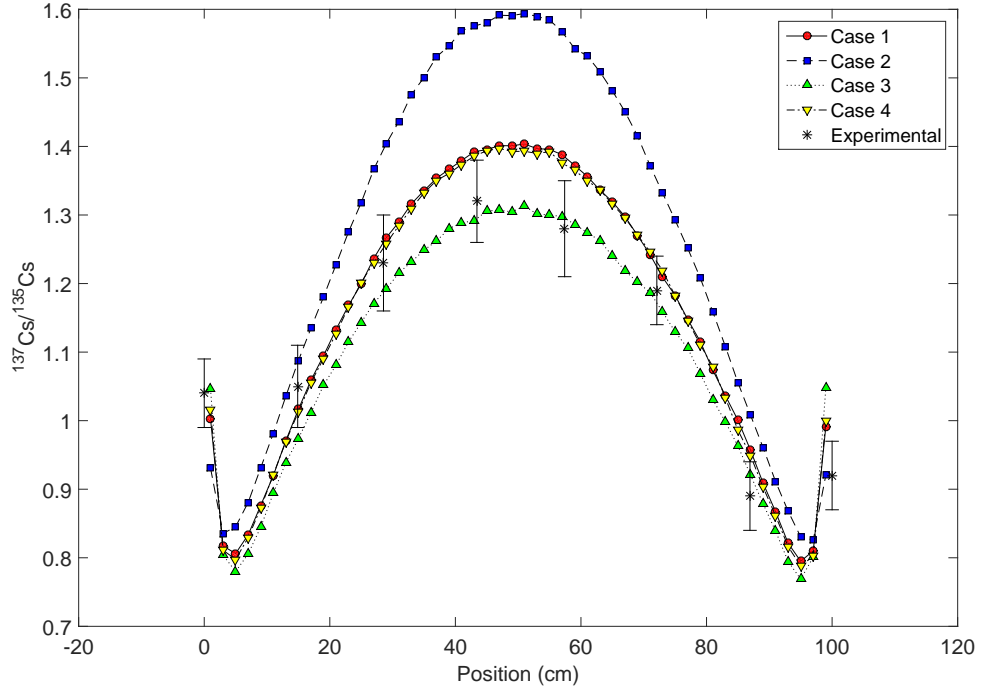
Figure 14: ^{137}Cs/^{135}Cs ratio for the four cases of ROI position

to be around the same point with some fluctuations. On average, higher boron concentration values reported lower values for the two ratios. The ratio of thermal (up until 0.5 eV) to epithermal (from 0.5 eV to 100 keV) neutron flux, shown in Table 6, decreased with increasing boron concentration. As the boron concentration increased, this effect increased the captures on ^{240}Pu relative to the number of captures on ^{239}Pu, which resulted in a net decrease in the ^{240}Pu/^{239}Pu ratio. Similarly, the ^{137}Cs/^{135}Cs ratio decreased due to the fewer captures on ^{135}Xe and therefore an increase in the relative ^{135}Cs concentration.

4.2 Uncertainty Analysis

The uncertainty analysis was approached in separate fashions for the rod position and boron concentration. The boron concentration affects the core on a macroscopic level; each cell of water in the model contains the same concentration of boron.

27
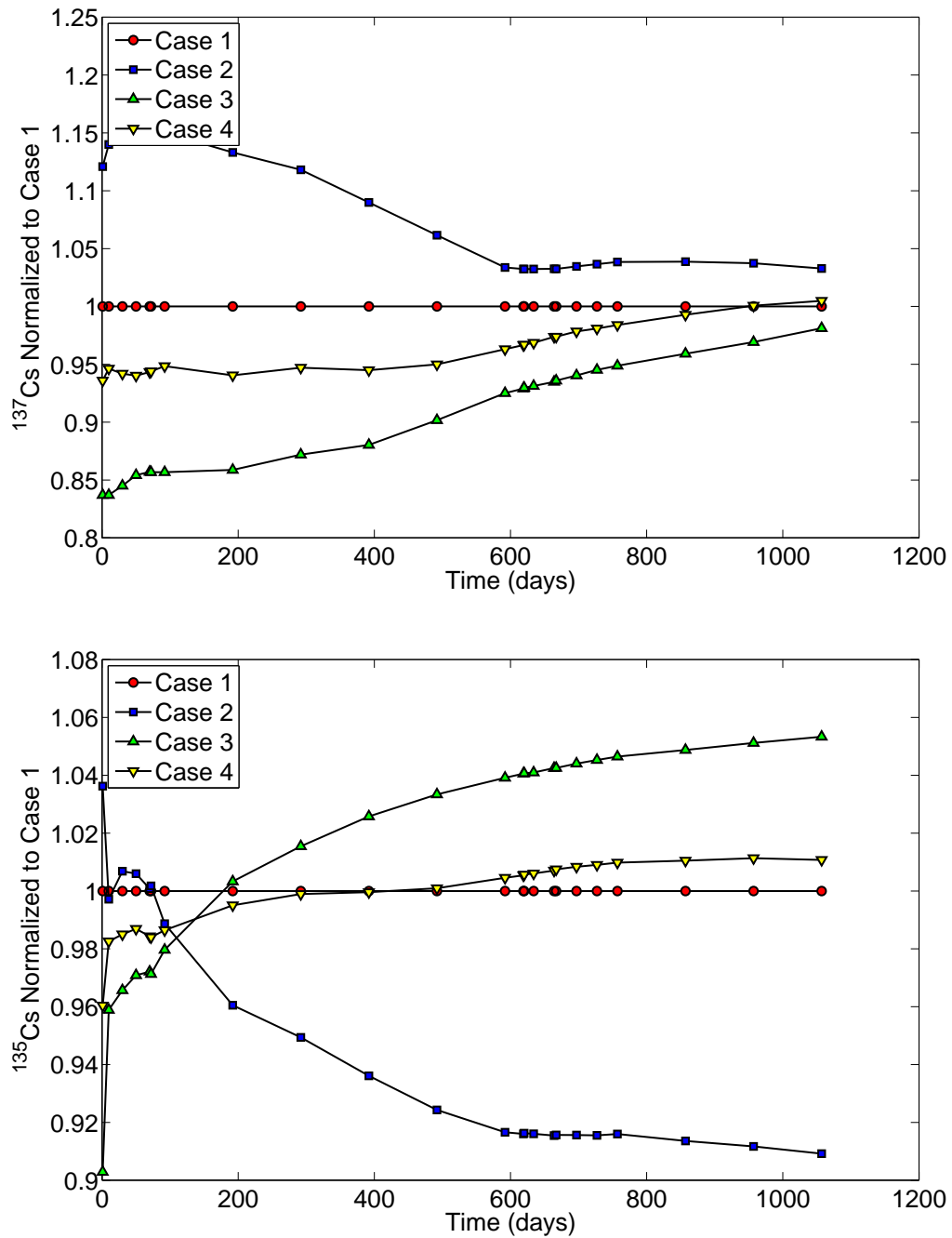
Figure 15: ^{137}Cs (top) and ^{135}Cs (bottom) concentrations relative to case one versus irradiation time

Therefore this macroscopic boron concentration is assumed to have a linear effect on the ratios in each axial cell, which makes the uncertainty simple to calculate. The rod
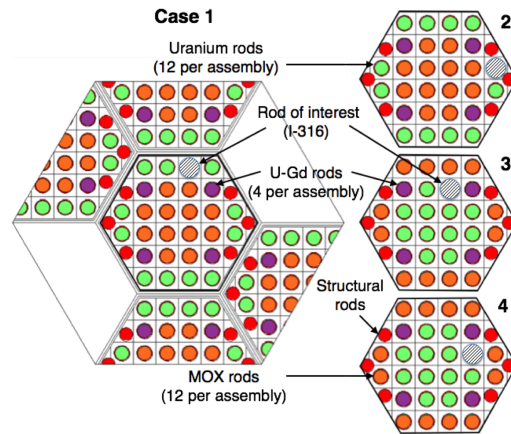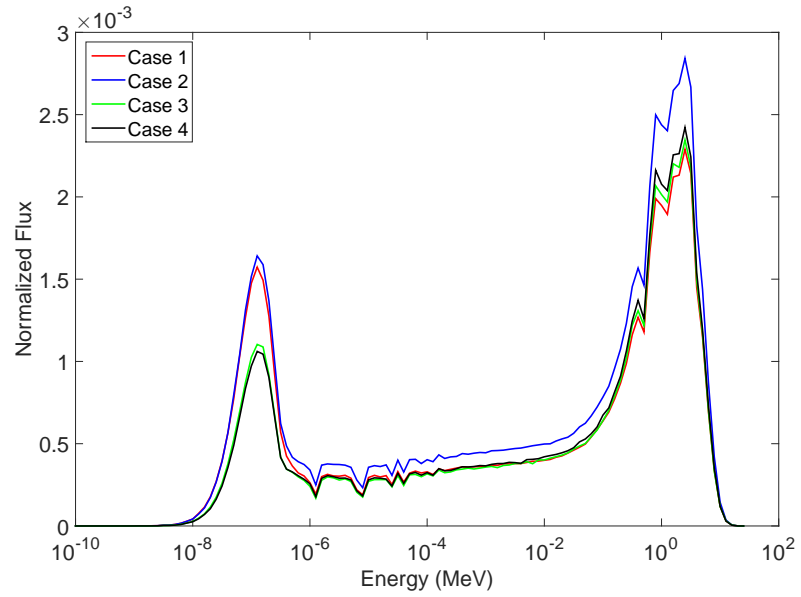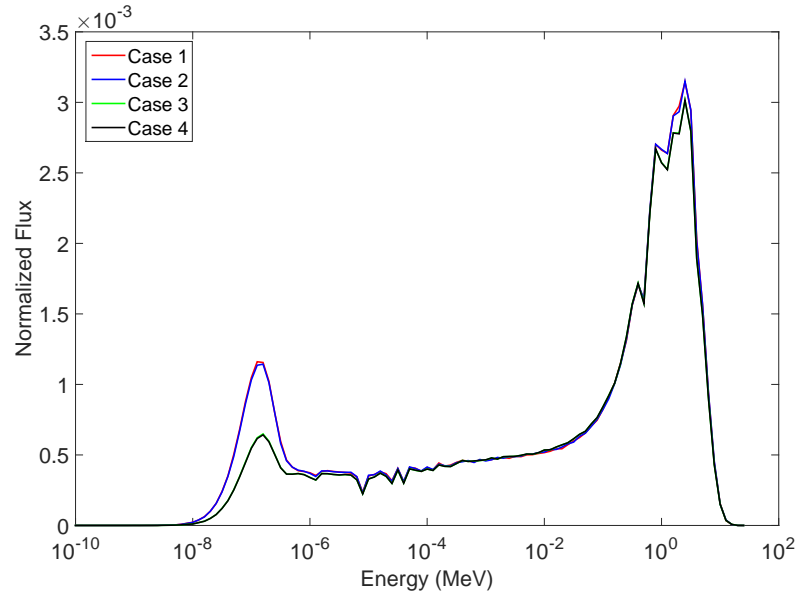
Figure 16: Neutron flux spectrum at the center of the rod at BOC (top) and EOC (middle) with assembly map of rod position cases (bottom)
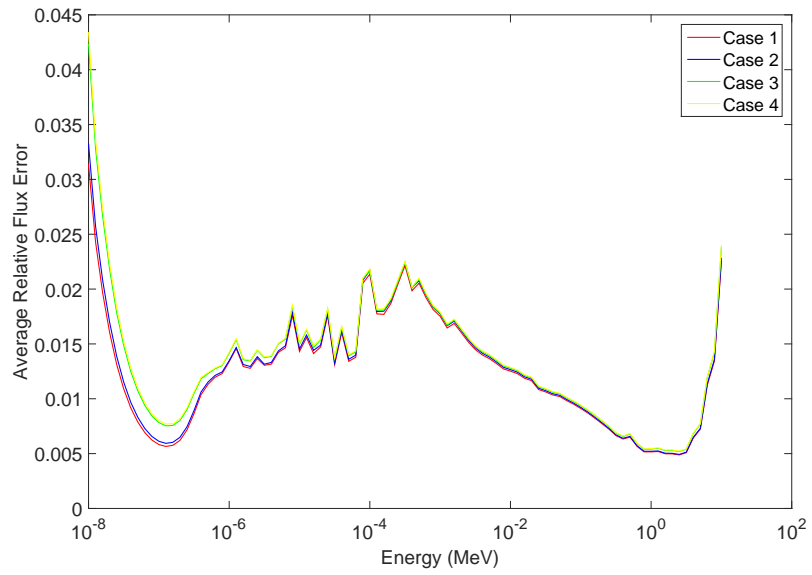
Figure 17: Average of all flux tally errors by energy group for an axial slice at the center of the rod
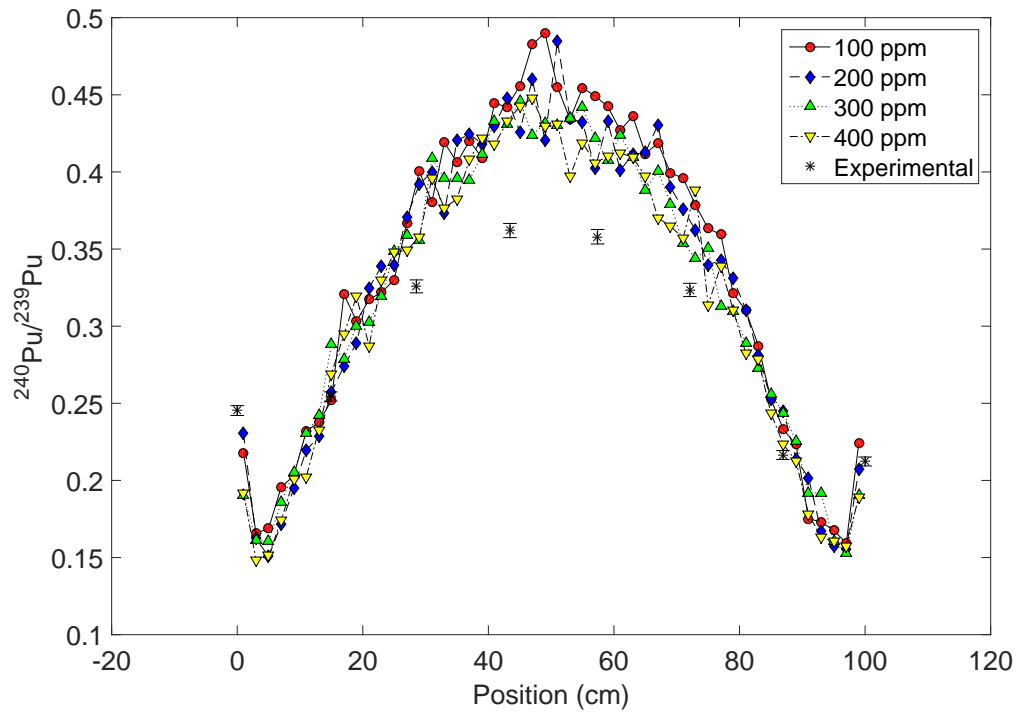
Figure 18: ^{240}Pu/^{239}Pu ratio for the four cases of coolant boron concentration
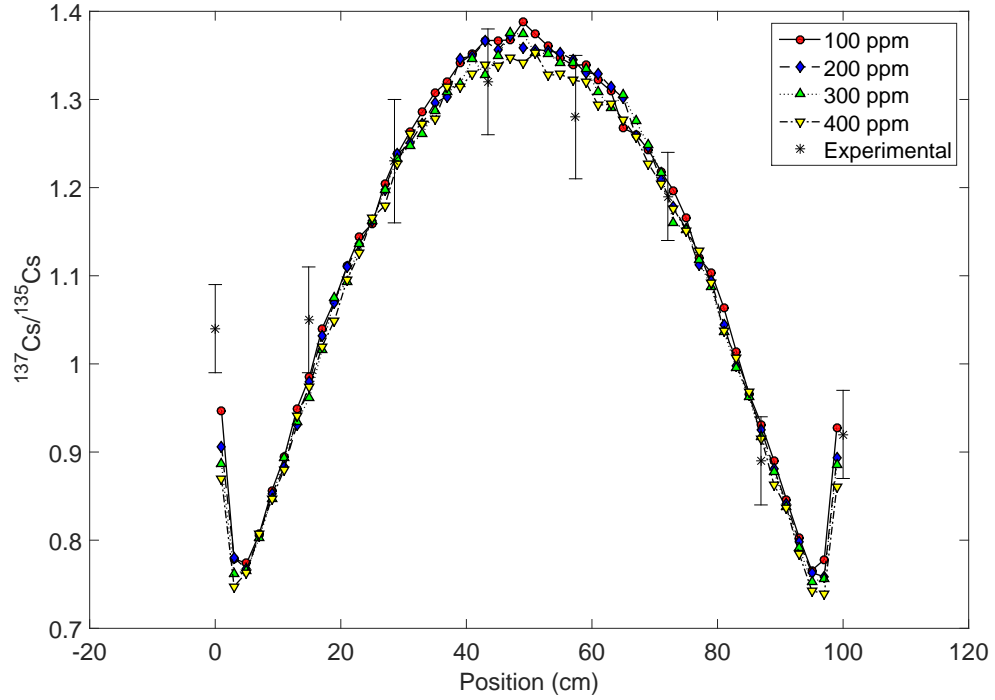
Figure 19: ^{137}Cs/^{135}Cs ratio for the four cases of coolant boron concentration

Table 6: Ratio of thermal/epithermal flux and axially-averaged ratios for boron concentration cases

Boron Concentration (ppm)	Thermal/ Epithermal Flux	Average ^{240}Pu/^{239}Pu	Average ^{137}Cs/^{135}Cs
100	0.851	0.334	1.125
200	0.802	0.327	1.119
300	0.794	0.322	1.113
400	0.775	0.317	1.107

position, however, is not a straightforward parameter; the isotope inventory depends on the flux due to the composition of material surrounding the ROI. A novel method for quantifying the rod position uncertainty is described below. For both parameters, the isotope concentration was analyzed as a function of the input parameters; these functions were assumed to be linear and independent of the other parameter(s).

4.2.1 Rod Position

It was necessary to calculate the systematic uncertainty of the position parameters due to the lack of information of the rods within the assembly of interest. An approximate error for the position parameters was be calculated with some assumptions. The first was that a linear response function quantifies the behavior of isotope inventory due to changes in nearby material in which neutron reactions are highly important (e.g. fissile and moderating material). The second was that the response function is only dependent on the nearby material at beginning of cycle (BOC), i.e. the flux behavior over time that result in a specific ROI isotope inventory were built into the function itself.

Each isotope final concentration was then viewed as a response function of the variables in the position parameter $\vec{x}$, which were defined as the types of rods in a unit cell volume surrounding the ROI. It was formulated that the variables that make up this parameter are the UO_2 rods, MOX rods, U-Gd rods, and water "rods" in a unit cell surrounding each axial slice of the ROI. In other words:

$$I_n = \sum_{i=1}^{4} A_{ni} x_i = A_{n1} U_n + A_{n2} P u_n + A_{n3} G d_n + A_{n4} W_n$$

Here, the four variables are the number of rods (UO_2, MOX, U-Gd, and H_2O respectively) in a unit cell of the eight closest rods surrounding the ROI. For clarity, a "water rod" exists when none of the other three rod types exists at one of those eight locations. As an example, the surrounding square shown in Figure 20 contains 1.5 UO_2, 1 MOX, 0.5 U-Gd, and 0 H_2O rods. The goal is to solve the matrix equation:

$$\vec{I} = \mathbf{A}\vec{x}$$

where the isotope vector $\vec{I}$ is the final inventory for isotope I_n for the four cases:

$$\vec{I} = \begin{bmatrix} I_1 \\ I_2 \\ \vdots \\ I_n \end{bmatrix} = \begin{bmatrix} I_{239Pu} \\ I_{240Pu} \\ I_{137Cs} \\ I_{135Cs} \end{bmatrix}$$

and

$$\vec{x} = \begin{bmatrix} U \\ Pu \\ Gd \\ W \end{bmatrix}$$

This matrix of coefficients of **A**, described previously, can be thought of as the coefficients of a variance-covariance matrix:

$$\Sigma^I = A \Sigma^x A^T$$

Using the coefficients of the response function as the partial derivatives of the response function with respect to each type of surrounding rod, the variance equation was reduced to its scalar form for each isotope response:

$$\sigma_{I_n}^2 = \left(\frac{\partial I_n}{\partial U} \right)^2 \sigma_U^2 + \left(\frac{\partial I_n}{\partial Pu} \right)^2 \sigma_{Pu}^2 + \left(\frac{\partial I_n}{\partial Gd} \right)^2 \sigma_{Gd}^2 + \left(\frac{\partial I_n}{\partial W} \right)^2 \sigma_W^2$$

$$+ \sum_{i=1}^{4} \sum_{j \neq i} \left(\frac{\partial I_n}{\partial x_i} \right) \left(\frac{\partial I_n}{\partial x_j} \right) \sigma_i \sigma_j \rho_{ij}$$

where i and j are U, Pu, Gd, and W (water) rods.

The values for the "coefficient" terms, the terms with the partial derivatives, were evaluated from the simulations of the four ROI position cases. The calculation of the standard deviation of the number of rods was performed with the assumption of quarter-symmetry within the assembly. When quarter-symmetry of rods within

Color	Rod Type
Yellow	ROI
Green	UO$_2$
Orange	MOX
Purple	U-Gd
White	H$_2$O
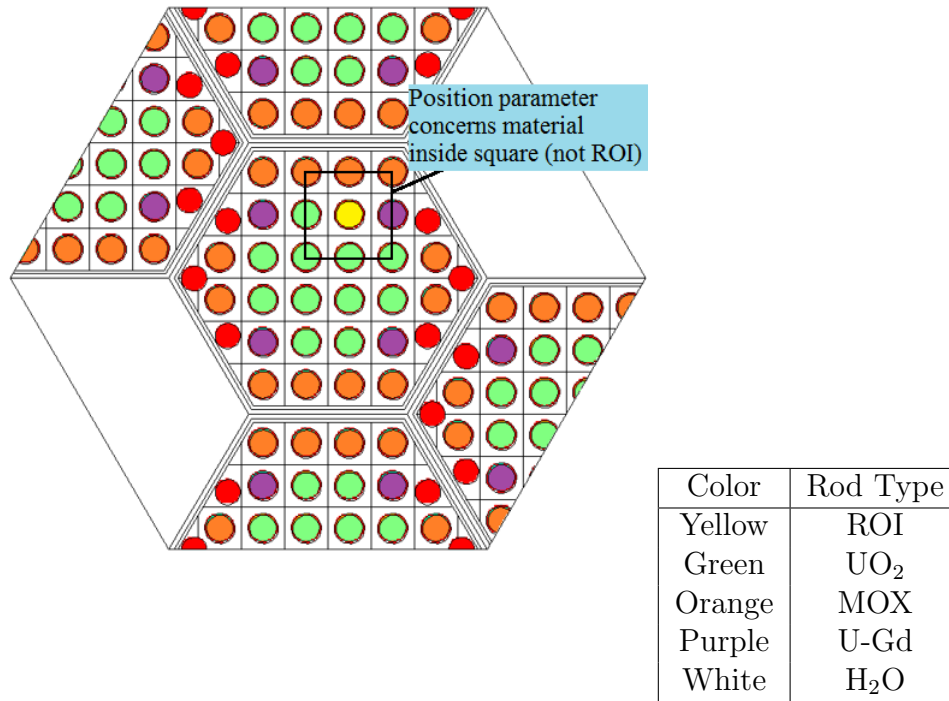
Figure 20: Position parameter represents the number of rods inside the square surrounding the ROI

the assembly was assumed, there existed only 85 configurations of rods within the assembly. A script was created to iterate through all of the possible combinations of rod configurations and determine the standard deviation of the number of each type of rod surrounding the ROI. The results are shown in Table 7.

To compare the results to the isotope ratios, the error for the plutonium and cesium isotopes were calculated using the propagation of error formula for the quotient

Table 7: Average and standard deviation of the number of surrounding quarter-rods by type (12 total in surrounding 8 rods)

Rod Type	Average Number in Surrounding Area (Quarter Rods)	Standard Deviation (Quarter Rods)
U	5.01	± 2.20
Pu	3.79	± 2.37
U-Gd	1.05	± 1.13
H$_2$O	1.93	± 2.05

of two function:

$$\sigma_{I_n/I_m}(z) = \frac{I_n(z)}{I_m(z)}\sqrt{\left(\frac{\sigma_{I_n}}{I_n(z)}\right)^2 + \left(\frac{\sigma_{I_m}}{I_m(z)}\right)^2 - 2\frac{\sigma_{I_n}\sigma_{I_m}\rho_{mn}}{I_n(z)I_m(z)}}$$

The uncertainty was calculated as a function of axial position within the rod of interest as the equation above relied on an axial-dependent isotope concentration. Neglecting the axial ends of the rod, the uncertainty of the ^{240}Pu/^{239}Pu ratio due to the variance in the unit cell composition was found to be in the range of 17-36% and the uncertainty of the ^{137}Cs/^{135}Cs ratio is found to be in the range of 7-15% (neglecting the axial ends). Tables with the uncertainties for the four cases of rod position are shown in Appendix A.

The results for the two ratios are plotted for case one in Figures 21-22; all of the other cases produced isotope ratio uncertainties similar to case one. These error bars were calculated from the propagation of uncertainty in the composition of rod types in the unit cell, which means that the error bars were interpreted as the uncertainty in the isotope ratio due to where that case falls in the phase space of unit cell composition. The plutonium ratio can be seen to have higher uncertainty than the cesium ratio. Despite the smaller change in the ^{240}Pu/^{239}Pu ratio from the sensitivity analysis, the error proved to be large as the quantity of each isotope changed appreciably from case to case. For the cesium ratio, the relative errors were much lower and they overlapped with all experimental points. These figures show a higher relative error at the axial ends, which makes sense due to their lower neutron population there, i.e. higher sensitivity to perturbation in neutron flux.

4.2.2 Boron Concentration

The effect of the uncertainty in the ratios due to the variance in the boron concentration was analyzed. Because the boron concentration is found to be a macroscopic effect, a simple propagation of error was performed. The response function of the
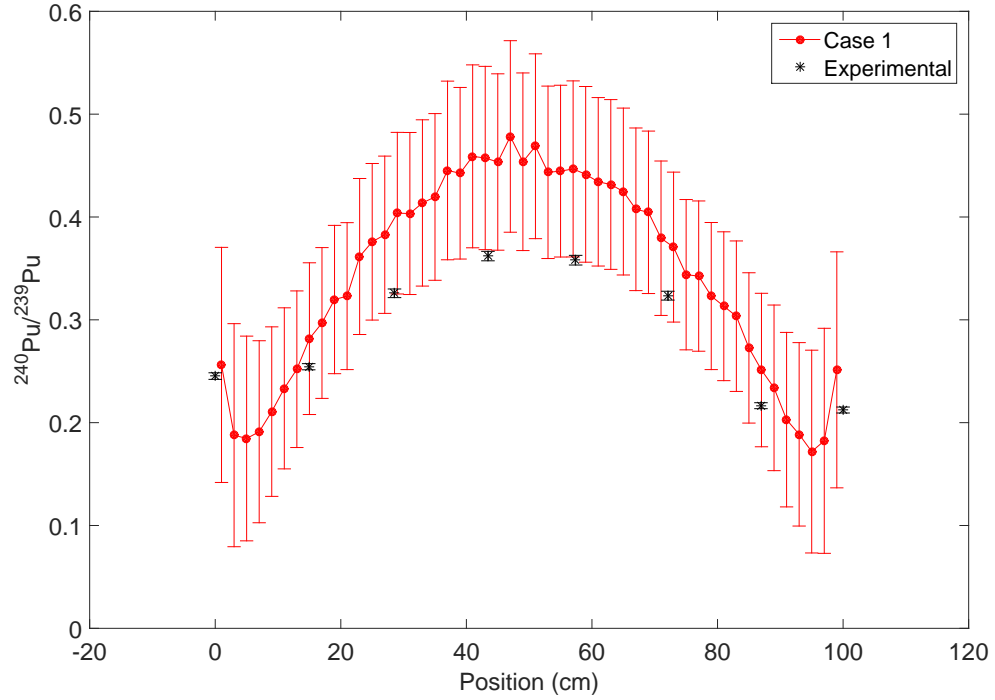
Figure 21: ^{240}Pu/^{239}Pu ratio with calculated rod position uncertainty for case 1

isotope ratio to the change in boron concentration again was assumed to be linear and of the form:

$$I_n(z) = A_B(z)B$$

where I_n is the isotope concentration at some axial position z, $A_B(z)$ is a coefficient, and B is the macroscopic boron concentration. Then the uncertainty in isotope was written as:

$$\sigma^2_{I_n(z)} = \left(\frac{\partial I_n(z)}{\partial B}\right)^2 \sigma^2_B$$

Here, the partial derivative term is equivalent to the coefficient term in the previous term, but is shown for a simpler understanding of what the coefficient means.

The maximum, minimum, and average changes in the ratios with respect to the boron concentration of all the fifty axial slices are shown in Table 8. The maximum

36
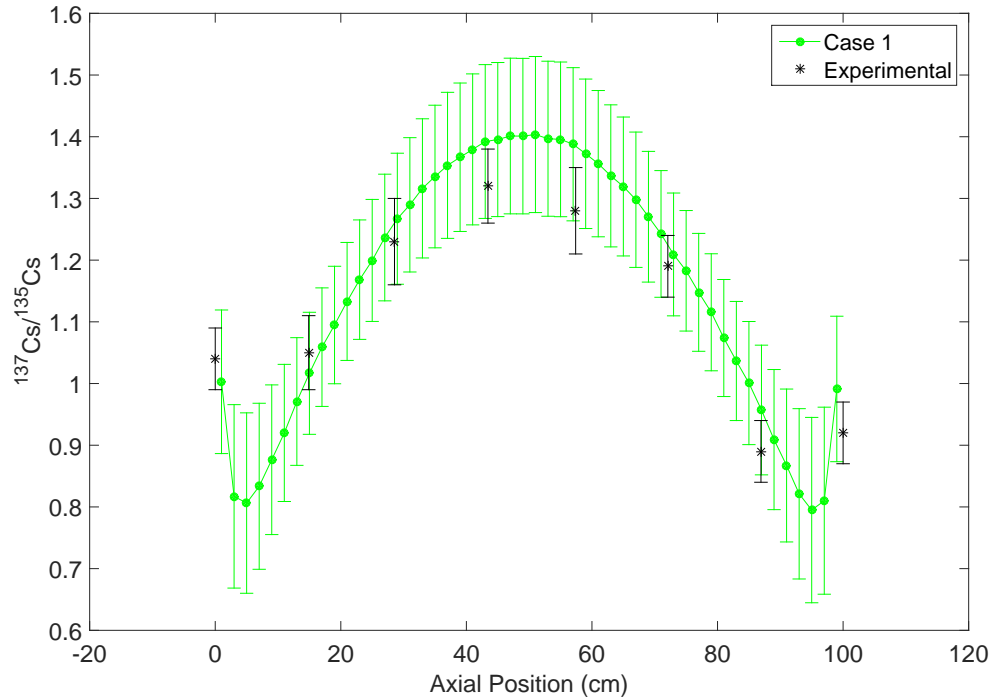
Figure 22: ^{137}Cs/^{135}Cs ratio with calculated rod position uncertainty for case 1

change for both ratios (neglecting ends of the rods) is plotted in Figure 23. This maximum response was the value used in the error analysis because it was the most conservative estimate of the isotope ratio uncertainty with respect to boron concentration. Note that it is plotted in absolute scale and not relative scale as each ratio changes upwards of 50% over the axial length.

The uncertainties in the ratios were calculated assuming an uncertainty of 200 ppm for the boron concentration in the coolant. The value of 200 ppm was chosen because the average boron concentration in the coolant for cycle 4A was approximately 250 ppm, yet the concentration for core 4A ranged from 0-450 ppm. For the maximum change in the isotope ratios, this calculation yielded a 8.7% change in the ^{240}Pu/^{239}Pu ratio and a 1.8% change in the ^{137}Cs/^{135}Cs ratio. For the average change in the ratios, this corresponds to a 4.4% change in the ^{240}Pu/^{239}Pu ratio and 1.2% change in the ^{137}Cs/^{135}Cs ratio. This change was negligible compared to the that presented by the

Table 8: Isotope ratio response to change in macroscopic boron concentration

$\partial\mathbb{R}/\partial B$ (ppm^{-1})	${}^{240}\mathrm{Pu}/{}^{239}\mathrm{Pu}$	${}^{137}\mathrm{Cs}/{}^{135}\mathrm{Cs}$
Maximum	1.75×10^{-4}	1.23×10^{-4}
Average	7.22×10^{-5}	6.52×10^{-5}
Minimum	1.07×10^{-6}	2.32×10^{-6}
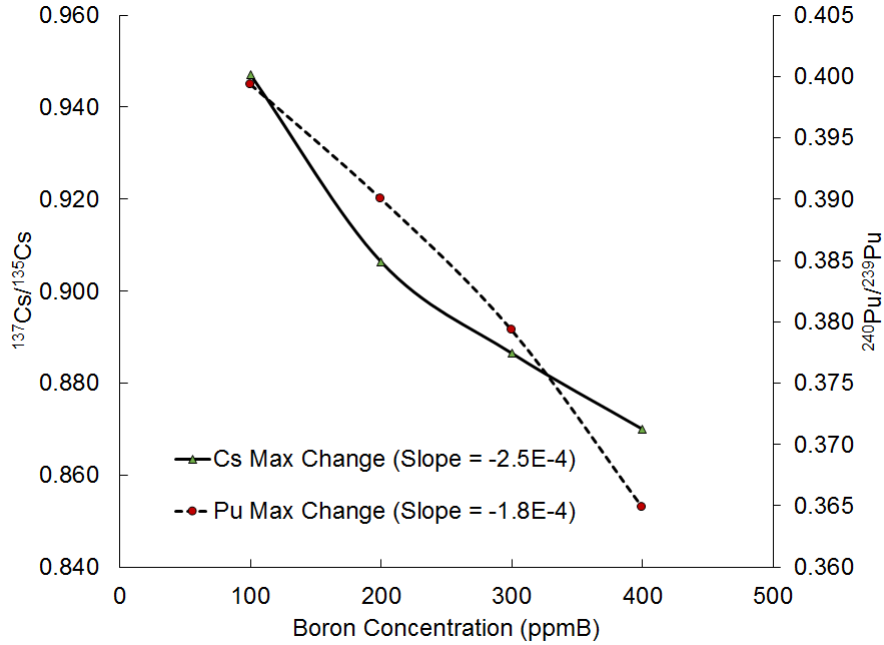
Figure 23: Maximum response of the ratios to the change in boron concentration

change in ROI position.

4.3 Expanded MCNP Model

The results for the sensitivity analysis revealed a mismatch between the experimental and predicted isotopes. The work discussed from this section onward examined this effect by changing MCNP input parameters and using simpler models. Much of this work could be further explored in the future by another graduate student.

A major simplification in the model was that all fuel materials of a certain rod type in the same axial slice contain the same fuel material; MCNP becomes difficult to run in practical time frames with many depletion materials. The consequences of this

should be minimal as this project focused on the axial distribution of isotope ratios. The model discussed up until this point had 200 fuel materials. Another model was created where each of the 88 fuel rods in the model had a different tracked material for each of the 50 axial slices, which amounted to a total of 4400 fuel materials.

When the expanded model is run in MCNP6, it became clear that it is not feasible to run MCNP with that many different fuel materials and many burn steps. Before finishing the first calculation of k_{eff} in the first time step, the MCNP runtpe file was at a size of 120 GB. That size is too large for practical simulation on a computer cluster.

Although the full model cannot be run, a single k_{eff} calculation can be performed, which is representative of the first time step in the model. An examination of this will be performed for different moderator lengths at the axial ends of the assemblies.

4.3.1   Length of Moderator at Axial Ends

The length of the moderator at the axial ends had a significant impact on the run time, and it changed the boundary conditions for the convergence of the flux. The length of the moderator is tested for five cases of moderator length above and below the modeled assembly. The five lengths are 10 cm, 5 cm, 2 cm, 1 cm, and 0.5 cm.

The normalized flux of each case for the rod of interest is shown in Figure 24. The normalized peak flux changed by a factor of approximately 8% from the 10 cm case to the 0.5 cm case. Further, the difference between the 5 cm case (the length of axial moderator used up to this point) and the 10 cm case was between 1-3% towards the center. These factors were did not explain a 30% difference between the experimental and predicted plutonium ratio.

The total flux as a function of radial position for different values of moderator length above and below the assembly of interest is shown for two different axial slices of the assembly of interest. Figure 25 and Figure 26 show the radial flux in the
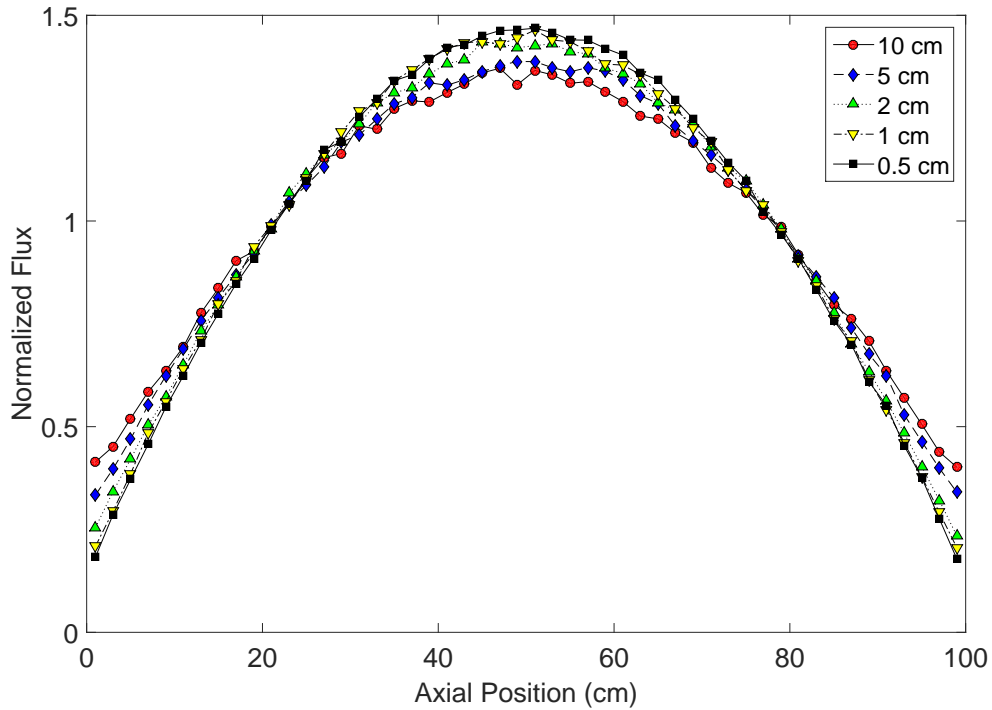
Figure 24: Axial shape of normalized flux for different cases of moderator length above and below the modeled assembly

assembly for the axial end slice and axial center slice, respectively. The cases shown in Figure 14 used a reflector length of 5 cm and are for case one of rod position (see Figure 11). These figures showed that the flux in the rods at the periphery was much higher than the MOX rods near the center.

For both axial slices, the flux map showed a much higher prediction for the flux for the rods at the corners of the assembly and that are surrounded by the most water. The rods located at the ends of the middle two rows experienced a much higher flux. Increasing the end moderator length from 2 cm to 10 cm increases the max peaking of these rods (relative to the other rods in the assembly) from 1.125 to 1.152 at the end and from 1.134 to 1.160 at the center.
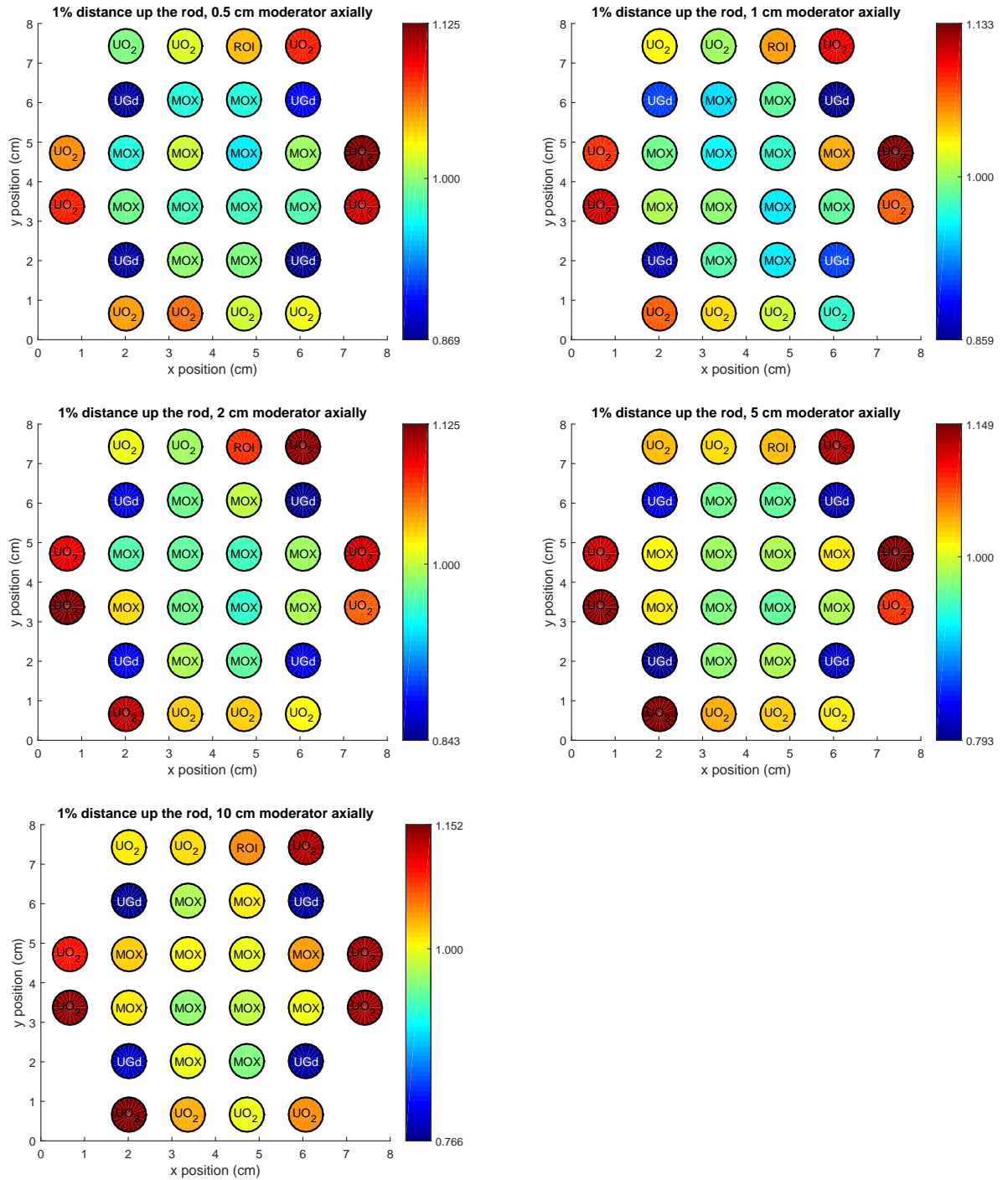
Figure 25: Flux at bottom slice (1% up the rod) for different length of axial moderator: 0.5 cm (top left), 1 cm (top right), 2 cm (middle left), 5 cm (middle right), 10 cm (bottom right) - Note: flux errors ranged from 1% to 2.5% at the axial ends of the rods
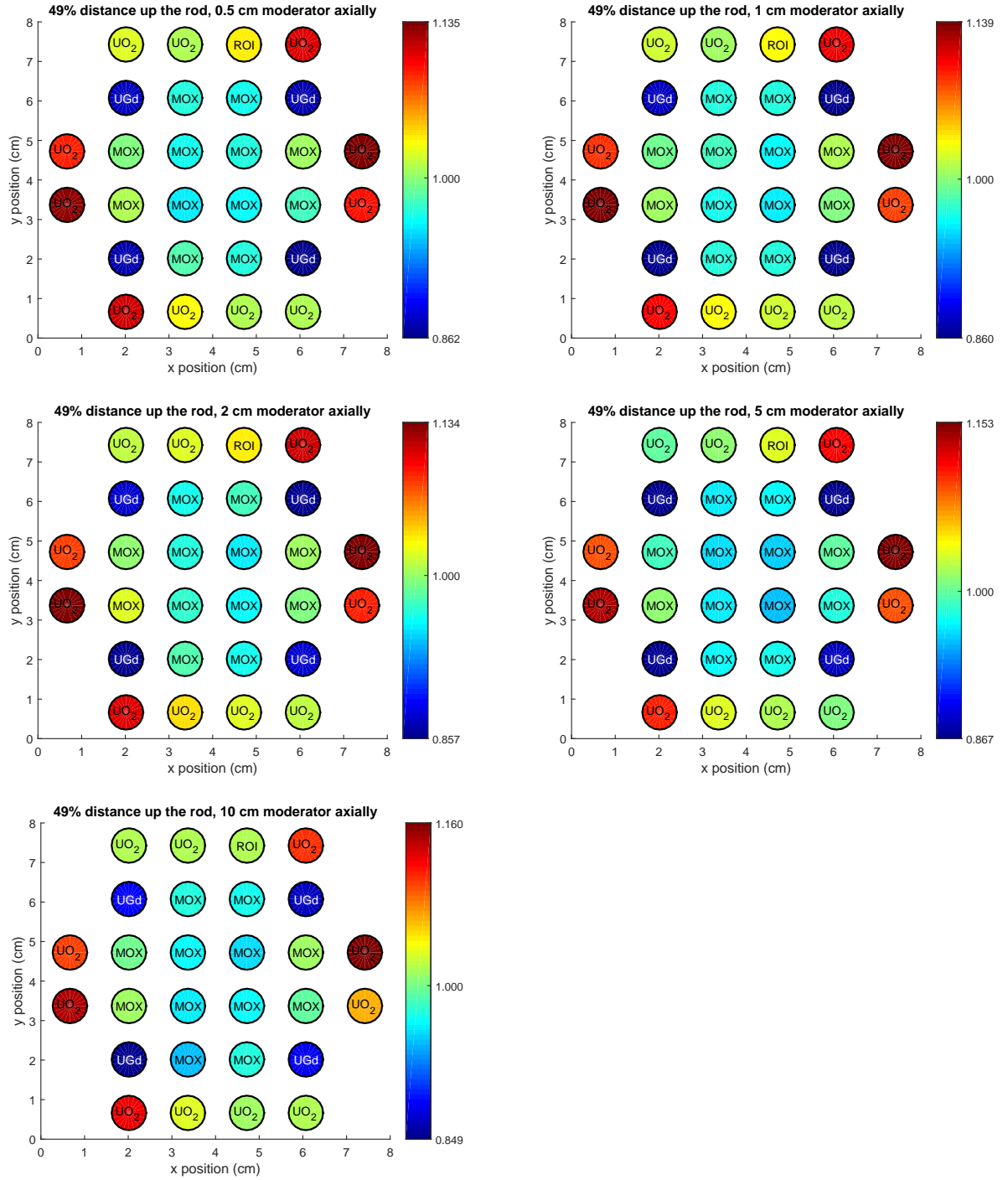
Figure 26: Flux at at middle slice (49% up the rod) for different length of axial moderator: 0.5 cm (top left), 1 cm (top right), 2 cm (middle left), 5 cm (middle right), 10 cm (bottom right) - Note: flux errors were less than 1% at the center of the rods

4.4 KCODE Input Changes

The number of source particles was initially inspected as a cause to the mismatch with experimental data. Their effect on the final ^{240}Pu/^{239}Pu and ^{137}Cs/^{135}Cs ratios is shown in Figures 27 and 28, respectively, when the source particle number was increased from 20,000 to 100,000. The cesium ratio was negligibly impacted by this increase in the number of source particles. The plutonium ratio, however, did noticeably decrease in statistical noise with a higher number of source particles. The number of source particles, however, had a minimal impact on the magnitude of the ^{240}Pu/^{239}Pu ratio and failed to explain the mismatch.

Then the number of source particles was increased from 100,000 to 1,000,000. The error of k_{eff} for 100,000 and 1,000,000 particles with 700 active cycles are shown in Figure 29. The time for the 100,000 and 1,000,000 particle cases to run one k_{eff} calculation were an order of magnitude in difference. Given that this calculation must be performed twice for each time step, once as "predictor" time step and once as a "corrector" time step, it was impractical to use the 1,000,000 source particles for 38 time steps. It was also decided to use only 200 active cycles instead of a larger number, such as 700. Using 700 active cycles would have increased the run time by a factor of ten but decreased the error by a factor of three, despite errors in flux and k_{eff} already being relatively small. A simulation with 1,000,000 source particles would not have finished completion in a time frame reasonable for this project as the simulations took approximately two weeks to perform with 100,000 source particles. For the sake of time and availability of computing resources on the LC clusters, 100,000 particles with 200 active cycles was deemed sufficient for these simulation purposes and found to have little impact on the magnitude of the ratios.
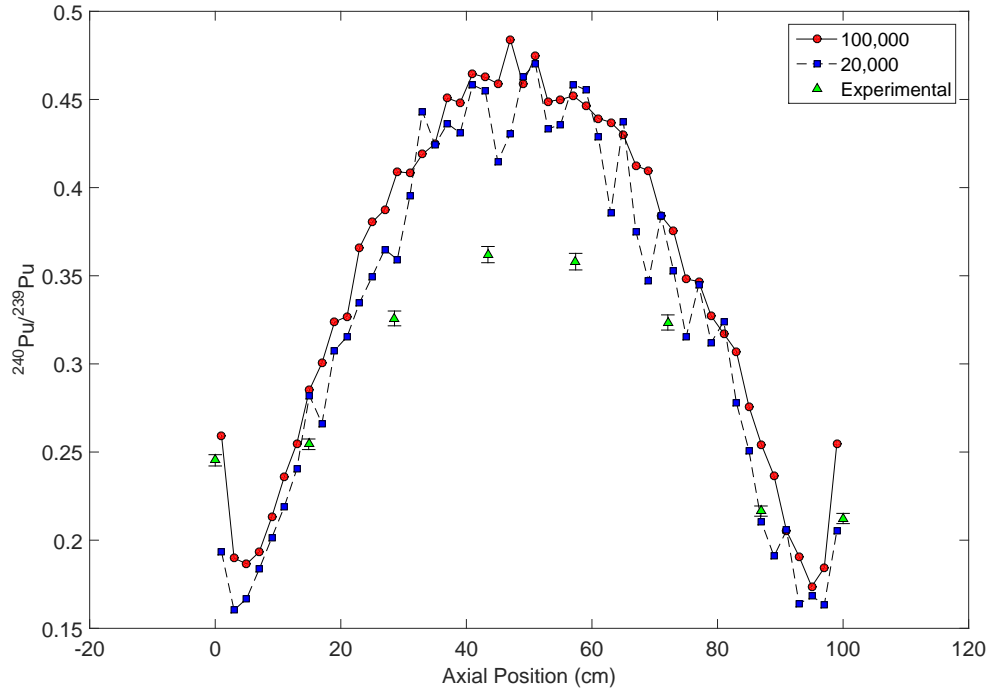
Figure 27: ^{240}Pu/^{239}Pu ratio comparison of using 20,000 vs 100,000 source particles for the full assembly model

4.5   Pellet Model

There is a clear disparity between the experimentally measured and MCNP-predicted ^{240}Pu/^{239}Pu ratio. A simple pellet model of the rod was created to test the effect of perturbations in MCNP input parameters on the plutonium ratio. The axial cross-section of the model, shown in Figure 30, consisted of a pellet that is 2 cm in height and of the geometry and side length equal to the pitch. All sides of the parallel-piped that contained the fuel pellet used the specular reflection boundary condition, i.e. this pellet was analogous to the axial center of a rod.

Figure 31 shows the ^{240}Pu/^{239}Pu ratio for the full assembly model (case one) versus the pellet model described above. The pellet model is run for separate powers with the same power history to obtain the "Pellet Model" series. The "Assembly Model" series represents all 50 axial locations for the ratio in the assembly model.
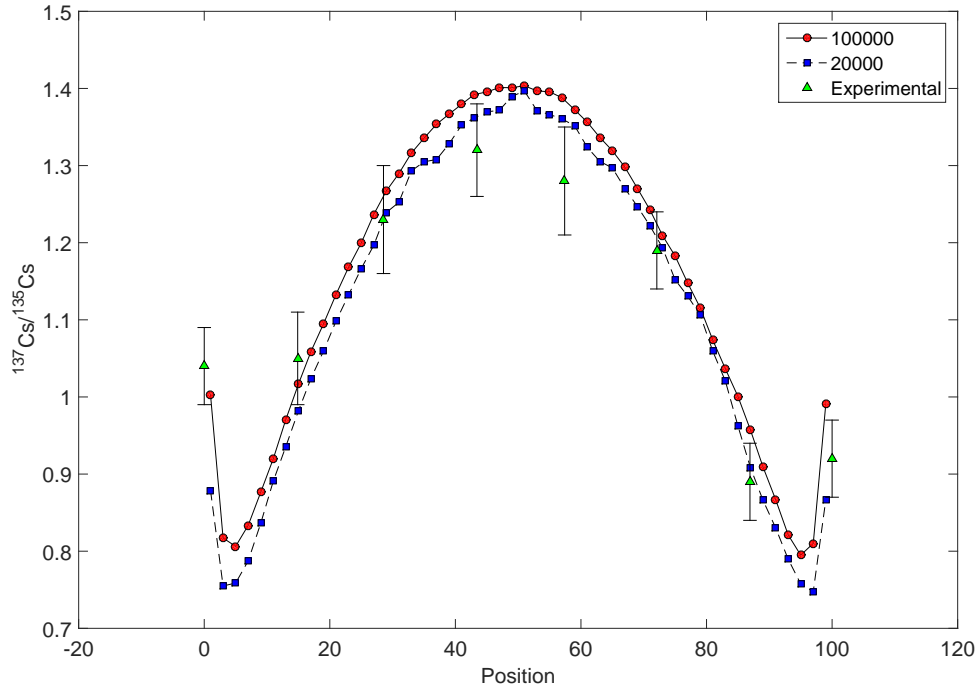
Figure 28: $^{137}Cs/^{135}Cs$ ratio comparison of using 20,000 vs 100,000 source particles for the full assembly model

This proves that there is a disparity between the pellet model and assembly model. The subsections below explore some of the reasons the initial assembly model was inaccurate.

4.5.1 Time Step Length

For criticality calculations in MCNP, the BURN card must be implemented. The BURN card arguments include a sequence of time durations (in units of days) for which to calculate the eigenvalue and flux distribution of the model. Due to the transient of ^{135}Xe, a significant neutron poison with a cross-section of 2.6 Mb, at the beginning of operation, small time steps were used when the model was increased from zero power. The effect of the length of the initial steps at each power uprate in the simulation was examined. Six cases were created with increasing number burn steps (and therefore calculation of the eigenvalue) at the beginning of operation. The

45
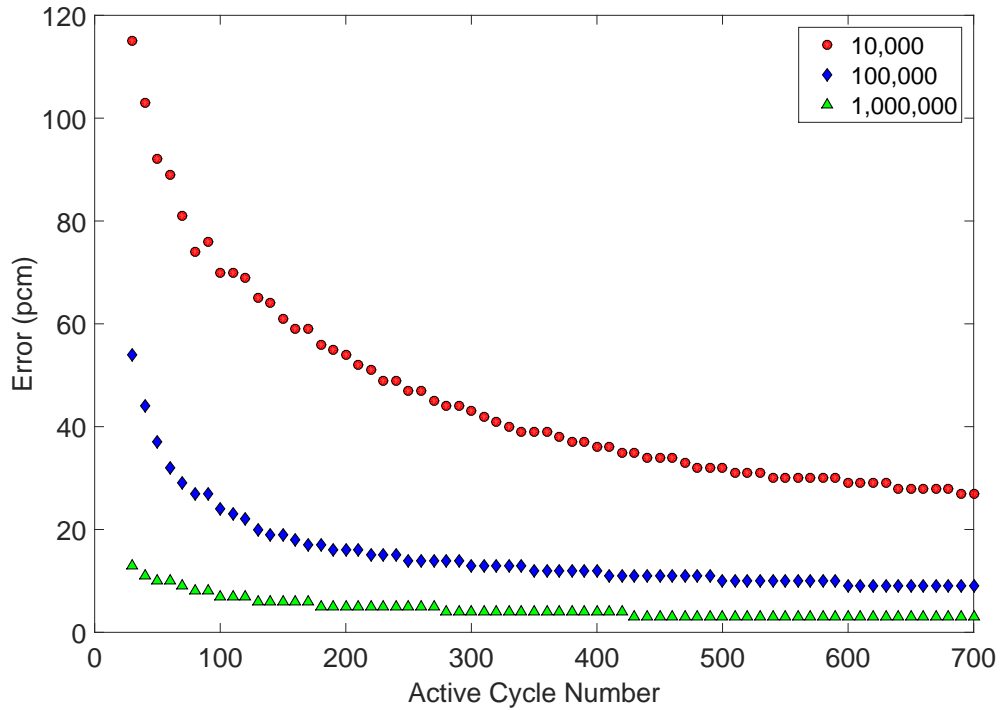
Figure 29: Error of eigenvalue by cycle for 100,000 and 1,000,000 source particles on KCODE
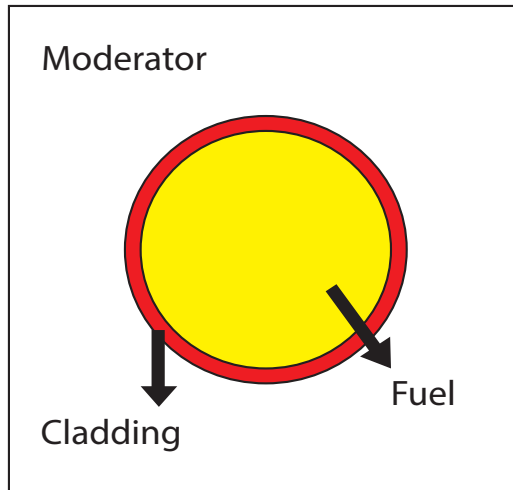
Figure 30: Axial cross-section of pellet model of BR3

step lengths of the first 73 days of each model are shown in Table 9.

The isotope inventory of ^{135}Cs, the isotope most affected by the xenon equilibrium, is shown in Table 9. All of the cases besides case one predicted ^{135}Cs with an RSD of 0.028% at 13 days and 0.011% at 73 days. The ^{135}Cs amount predicted case one was
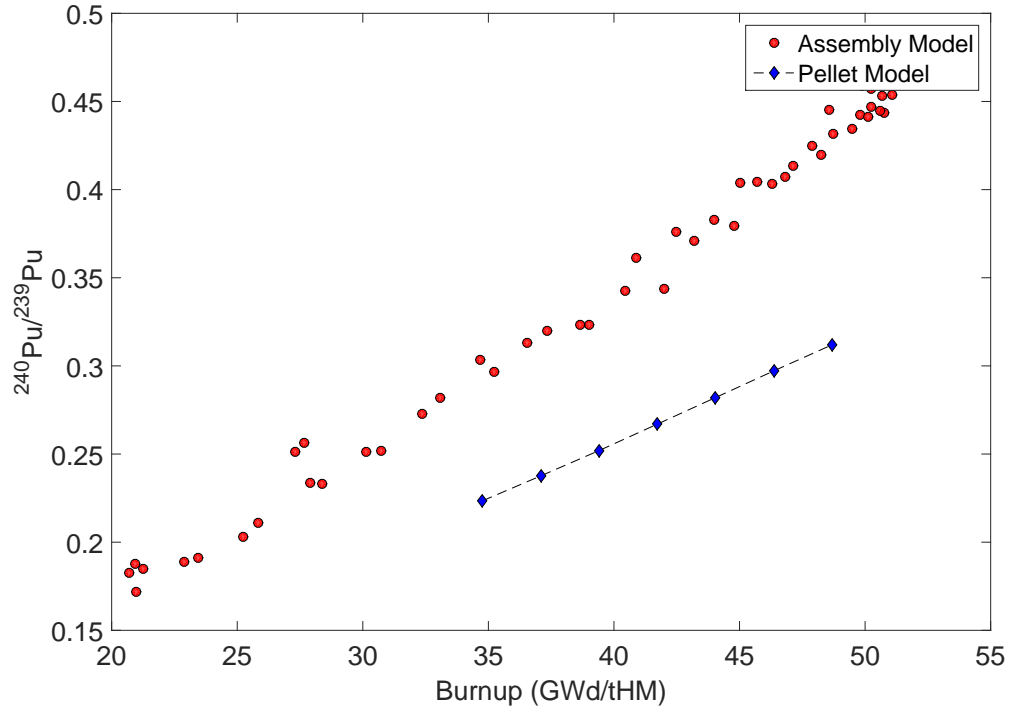
Figure 31: Comparison of ^{240}Pu/^{239}Pu ratio against burnup for pellet model and full model (Case 1 of Figure 11)

predicted 2.0% above the average of the other five cases at 13 days and 0.37% at 73 days. In addition, the ^{137}Cs had similar statistics.

The final plutonium and cesium isotopes (after the 30 year cooling time) changed insignificantly amongst the runs. None of the relative standard deviations of the final isotope concentrations was higher than 0.18%. This finding suggested that the time step intervals used in modeling transients had an insignificant impact on prediction of theses isotopes towards the axial center of an assembly, particularly when large time steps of constant power existed later in the model.

4.5.2 Number of Shutdowns

The number of shutdowns has a significant impact on the isotopic composition in the fuel. With each shutdown, some actinides and fission products decay. When a

Table 9: Pellet model cases with different step lengths at BOC for xenon equilibrium

Case	Day to calculate isotope inventories (first 73 days of burn)
1	13 73
2	3 13 73
3	0.5 1.5 3 13 73
4	0.25 1 3 13 73
5	0.1 0.4 1 1.75 3 13 73
6	0.1 0.3 0.6 1 1.5 3 13 73

shutdown occurs, most of the ^{135}Xe decays directly to ^{135}Cs because there is insignificant competition from the neutron absorption when the reactor is shut down. When the number/length of shutdowns is unknown, this can add more uncertainty to the measurement, particularly the ^{137}Cs/^{135}Cs ratio. The ^{137}Cs concentration will also decay with large shutdown times and cooling time after discharge from the reactor.

Pellet models were created with varying number of shutdowns. The length for all shutdowns was set to 30 days. As expected, the number of shutdowns had little impact on the ^{240}Pu/^{239}Pu ratio. The ^{137}Cs/^{135}Cs ratio decreased with an increasing number of shutdowns. This decrease had little to do with the ^{137}Cs decay (half-life of 30 years), and more to the jump in ^{135}Cs concentration due to the decay of ^{135}Xe to ^{135}Cs at zero power. Figure 32 shows that the drop is almost linear, assuming a 30-day shutdown. The smaller the fraction of the shutdown relative to the half-life of ^{135}Xe, the more severe the spike should be in ^{135}Cs.

4.6   SCALE Pellet Model

A similar pellet model was created in SCALE 6.1 to compare the isotope differences. The T6-DEPL sequence and KENO-VI were used, which were necessary for 3D Monte Carlo calculations in SCALE. In SCALE 6.1, the continuous energy cross-section library for ENDF B-VII.0 (ce-v7-endf) was not available with the T-DEPL
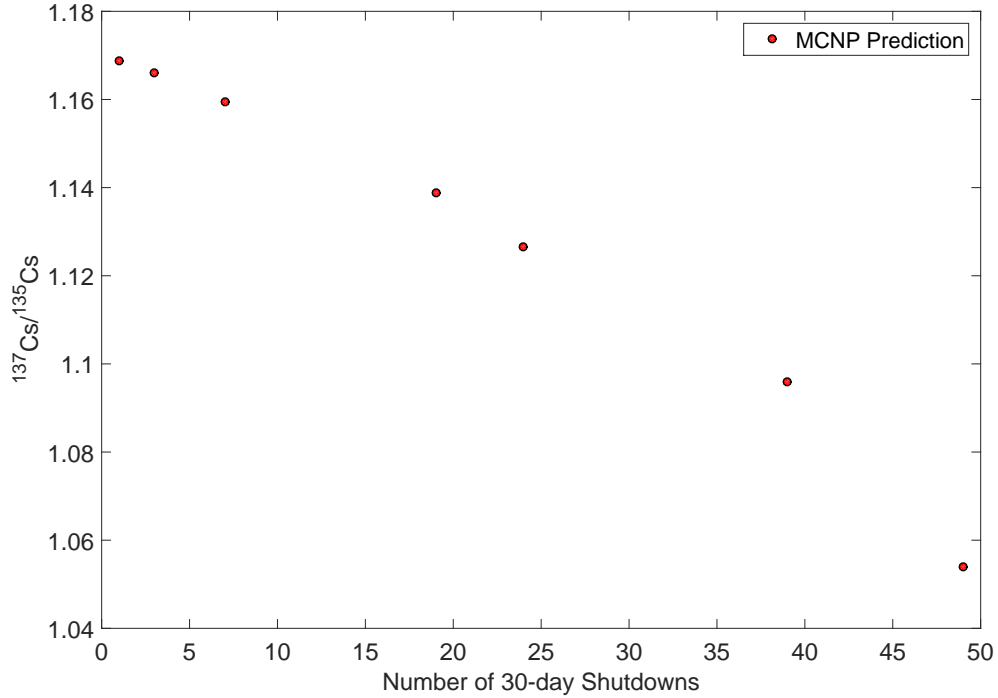
Figure 32: Number of shutdowns in the pellet model versus the ^{137}Cs/^{135}Cs ratio

sequences. Therefore the 238-group cross-sections were used (v7-238). All the material compositions, geometry, and power steps were created to be the same as in the MCNP pellet model.

Because MCNP/KCODE/BURN and SCALE/KENO/T-DEPL are stochastic codes, several runs of the pellet models were run to ensure that the isotope concentration after the power history and decay did not change much for each code. Five runs with different random number seeds were created to quantify this change. Table 10 shows the relative standard deviation (RSD) of each final isotope concentration among the five runs. Because these RSDs are so low, it was justified that using one single simulation of each would suffice.

Because the results for the MCNP assembly/pellet models showed a disparity between the ^{240}Pu/^{239}Pu ratio and burnup, the SCALE pellet model had the opportunity to verify the pellet models. However, the results from Figures 33 and 34 show

Isotope	SCALE Relative Standard Deviation (RSD)	MCNP Relative Standard Deviation (RSD)
^{135}Cs	0.0118%	0.0000%
^{137}Cs	0.0000%	0.0076%
^{239}Pu	0.0504%	0.0188%
^{240}Pu	0.0447%	0.0655%

Table 10: Relative standard deviation (RSD) of final isotope concentrations at the end of depletion simulation of pellet models with five different random number seeds

that the ratios of interest were similarly predicted as a function of burnup. The slight shift in the lines could be of interest to a future study. Overall, the difference between MCNP and SCALE was relatively small (only a few percent) compared to the disparity presented by the assembly model. This finding suggested that the approach to modeling the assembly model may have been incorrect, or that the true configuration of rods within the assembly was not tested.

The ratio of isotope concentrations for the MCNP and SCALE pellet models is shown in Figure 35. It can be seen that MCNP was under-predicting the plutonium and cesium isotopes but over-predicting the uranium content. However, the ^{240}Pu/^{239}Pu ratio being far off in the assembly model could not be explained by the discrepancy between MCNP and SCALE. The ratio of ^{240}Pu/^{239}Pu of MCNP to SCALE is not significantly off from unity.
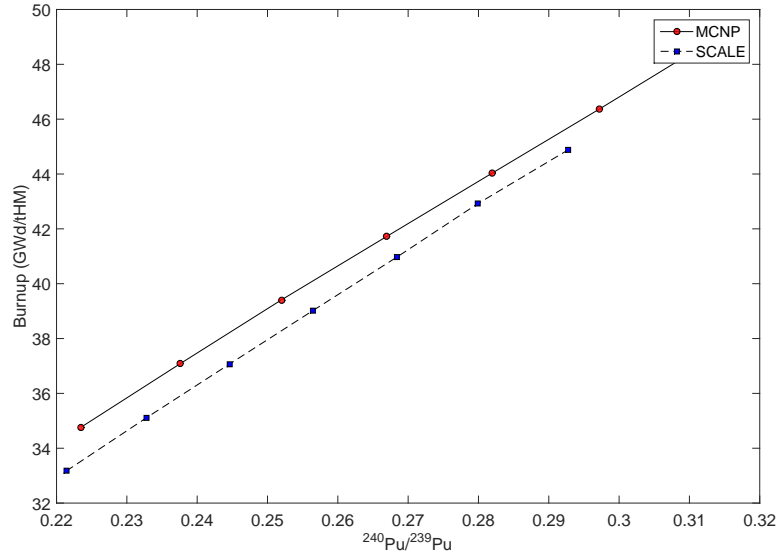
Figure 33: Comparison of ^{240}Pu/^{239}Pu versus burnup for MCNP and SCALE pellet models
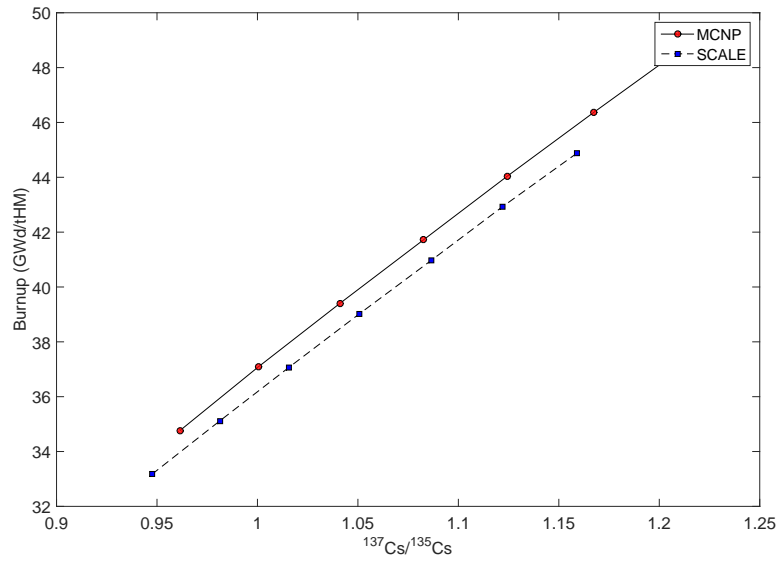
Figure 34: Comparison of ^{137}Cs/^{135}Cs versus burnup for MCNP and SCALE pellet models
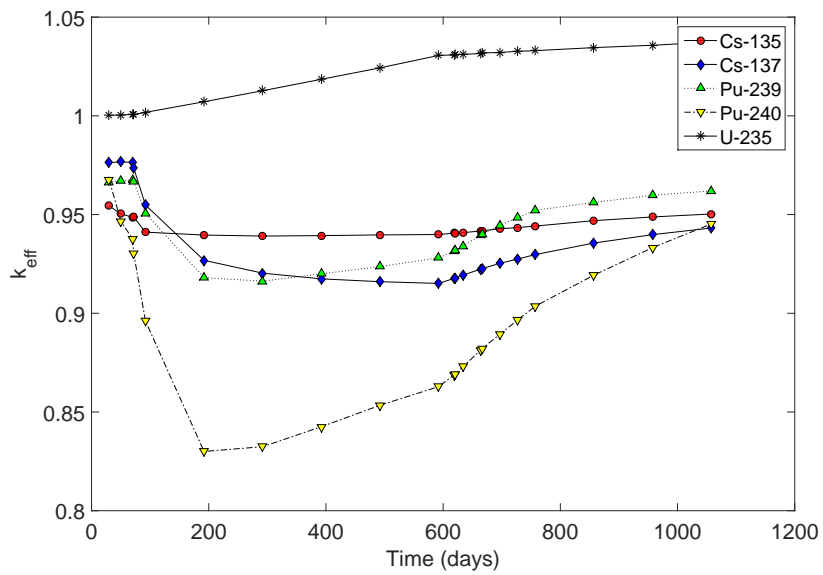
Figure 35: Ratio of MCNP/SCALE predicted isotopes as a function of reactor irradiation time

CHAPTER V

CONCLUSIONS

The goal of this work was to analyze the uncertainty of operating parameters on the ^{240}Pu/^{239}Pu and ^{137}Cs/^{135}Cs ratios. The work was performed on this reactor because experimental data of these ratios in a rod from the BR3 reactor core 4A/B was available. Despite that, there was a large lack of information about the reactor operation, including: rod position, assembly configuration, control rod insertion lengths, etc. An important note is that it was nearly impossible to gain solid evidence of rod location only due to studies of a few assembly configurations. In addition, the computational and experimental values did not agree well. However, many conclusions about the behavior of ^{240}Pu/^{239}Pu and ^{137}Cs/^{135}Cs ratios were drawn from this work.

Rod location was one of the primary focuses of this research and yielded unexpected results and more questions about its impact on the isotope ratios. Of the four test cases of the rod of interest (ROI) position, the ^{137}Cs/^{135}Cs ratio for case two was predicted by the model to be high compared to the other cases and experimental values. Case two had the ROI at the periphery of the assembly, where it would "see" a lot of water. The flux spectrum at that rod was much softer than that of the other cases. Case two, however, could not be ruled out as the plutonium and cesium ratios do not agree with respect to the experimental. The sensitivity analysis of the boron concentration found that a harder spectrum produced plutonium ratio results closer to the experimental. Effects that drive the flux spectrum to be harder could be examined in a future study.

The plutonium ratio was found to have higher statistical noise compared to the cesium ratio. This is due to their production methods in MCNP. Cesium isotopes

are fission products, which means that they will be a direct multiplication of the fissions that MCNP standardizes to match the power. Plutonium, on the other hand, is dependent on the capture on ^{238}U, a stochastic effect that does not depend on model-set power. Cesium therefore was seen to converge faster than the plutonium.

The uncertainty analysis found errors in the range of 17-36% for the ^{240}Pu/^{239}Pu ratio and 7-15% for the ^{137}Cs/^{135}Cs ratio, which quantifies how much the ratios could change due to a change in unit cell composition for a certain axial slice given a certain rod-average burnup. These systematic errors remained much larger than the experimental errors, which were 1.1-1.3% for the ^{240}Pu/^{239}Pu ratio and 4.2-5.7% for the ^{137}Cs/^{135}Cs ratio. The analysis also showed that changing the boron concentration had a minimal impact on the ^{240}Pu/^{239}Pu and ^{137}Cs/^{135}Cs ratios. Even though boron in the coolant has a larger relative impact on the thermal flux in a region with a softer spectrum, the ratios changed 8% at a maximum for the plutonium ratio and 1.8% for the cesium ratio.

The pellet model provided quantification to MCNP parameters associated with the prediction of these ratios. With a long power history and many complicated power steps, it was found that the length of the initial time steps in the MCNP models had a negligible impact on the final isotope ratios. These studied show how the number of source particles impacted the statistical convergence of the ratios. The number of shutdowns had an inversely linear proportionality with the ^{137}Cs/^{135}Cs ratio due to the large conversion of ^{135}Xe to ^{135}Cs with a drop in flux.

The agreement of the pellet models for SCALE and MCNP gives rise to questioning the results of the model when it is expanded to the assembly-level in MCNP. The assembly model has correct reactor geometries, material compositions, and cross-sections, therefore the reason as to the over-prediction of the magnitude of the ^{240}Pu/^{239}Pu ratio is still yet to be determined. Simulation inputs that were confirmed to being relatively independent of the problem included number of source

particles, length of time steps, cross-section libraries, and moderator length at the axial ends of the assembly. Many reasons could have contributed to the offset between experimental and computational, but most of note include the selection of only a few test cases and the large uncertainty in many of the reactor operating parameters.

The approach to modeling the assembly in MCNP did not match well with experimental data, yet uncertainty in reactor operating parameters played a vital role in understanding the exact behavior of isotopes in irradiated nuclear fuel. This conclusion implies that nuclear forensics has a difficult task in determining reactor operating parameters fuel composition as reactor models need low uncertainty to give accurate results. It is still necessary, however, to come up with these predictive models to verify experimental signatures as little could be known of intercepted radioactive material. Nuclear forensics must continue to invest in new techniques and measures to narrow uncertainty about fuel samples about which little information is known.

CHAPTER VI

FUTURE WORK

Because the plutonium ratio did not fully statistically converge, using more source particles or active cycles in MCNP could be used. In addition to that, an investigation of the disagreement of the computational and experimental should be explored. It does not make sense that the cesium appeared to match the experimental and the plutonium did not. A different code system, such as SCALE or SERPENT, could also be used to look at how the codes compare at the assembly level. Some work was done to explore this at the pellet level, however a SCALE model of the assembly could be created to explain some of the phenomena in this research.

The BR3 reactor operated at many different powers, the lowest of which was 48.6% of the full power. In order to operate at this power level, control rods must have been partially inserted into the core to decrease the power. The presence of the control rods will shift the neutron flux to a harder spectrum where they are inserted. Therefore control rods will have an effect on the power distribution and therefore isotope concentration, particularly at the axial top of the nearby rods.

Information on the surrounding assemblies of the assembly of interest and its orientation with respect to those surrounding assemblies of BR3 4A/B is information that was not available at the time of this research. Examining the orientation of the assembly of interest with respect to the water channels could also be investigated. The shuffling of assemblies should also be investigated as information was not available on the core shuffling of the BR3 between cores 4A and 4B.

The effect of the number of shutdowns and length of shutdowns in a full assembly model could be examined. During any shutdown or drop in reactor power, there

is a spike in the ^{135}Cs concentration due to the decreased flux and therefore fewer ^{135}Xe parasitic captures. This effect is important as the BR3 had many short scrams and several decreases in power. Because the number and length of shutdowns of a fuel sample could have high uncertainty, a quantification of this effect would provide valuable information to the field of nuclear forensics.

Some changes could have been made to improve the uncertainty analysis. First, using a simpler model, such as the unit cell (the ROI surrounded by its eight nearest neighbors), would have allowed for faster run time and the examination of more cases. The response function developed could also be exapnded to different types of rods, including control rods and rods with different levels of enrichment/fissile content. The cases used for the uncertainty analysis were those simulated for the sensitivity analysis. If repeated, bounding cases could have been chosen, e.g. the cases that might have experienced the softest and hardest spectra. With some additional cases between those two extremes, one could interpolate the behavior of the ratios.

Finally, the BR3 reactor core 4A/B had uncertainties in many of its input parameters. This posed a problem in trying to explain the behavior seen in the simulations. Therefore repeating this entire process for a sample that came from a reactor with more publicly available information. Examining the sensitivity and uncertainty for only one or two unknown input parameters would more likely produce meaningful results.

APPENDIX A

ROD POSITION UNCERTAINTY RESPONSE FUNCTION RESULTS

As described previously, the systematic uncertainty associated with the rod position is calculated as a function of axial position. They are shown below for the ^{240}Pu/^{239}Pu and ^{137}Cs/^{135}Cs ratios. Higher uncertainty exists at the axial ends of the rods because the population of these isotopes is smaller, therefore a similar perturbation in the flux will have a larger relative impact on the axial ends.

Table 11: Errors for the ROI position cases for the ^{240}Pu/^{239}Pu

Position (cm)	Case 1	Case 2	Case 3	Case 4
1	63.31%	74.53%	110.46%	73.09%
3	72.47%	80.77%	115.05%	80.87%
5	59.89%	73.94%	101.26%	65.11%
7	49.04%	54.26%	81.04%	52.90%
9	42.58%	43.34%	68.30%	47.42%
11	36.19%	37.19%	60.30%	43.66%
13	31.24%	30.54%	51.89%	35.90%
15	25.43%	26.52%	45.29%	27.21%
17	25.33%	23.46%	41.64%	30.52%
19	22.44%	21.22%	38.91%	25.99%
21	21.58%	19.65%	36.69%	26.40%
23	20.77%	18.15%	33.47%	25.04%
25	19.83%	18.36%	34.89%	23.64%
27	19.39%	16.99%	30.35%	23.53%
29	18.76%	16.91%	29.46%	21.26%
31	18.84%	17.03%	31.29%	22.84%
33	18.48%	16.90%	29.79%	19.35%
35	17.53%	16.95%	28.18%	19.19%
37	18.64%	17.16%	30.70%	22.83%
39	17.90%	16.90%	26.67%	19.16%
41	18.21%	16.84%	29.37%	18.64%
43	18.32%	16.43%	28.82%	19.40%
45	18.54%	16.95%	28.17%	23.21%
47	17.79%	17.35%	25.12%	22.07%
49	18.49%	16.98%	28.83%	19.33%
51	18.36%	16.78%	27.44%	20.53%
53	17.64%	16.79%	25.67%	21.49%
55	17.71%	17.28%	26.48%	19.46%
57	18.68%	17.03%	28.80%	20.37%
59	18.68%	17.13%	30.44%	19.59%
61	19.20%	17.13%	29.32%	23.50%
63	18.20%	16.90%	26.20%	22.88%
65	18.93%	16.45%	29.24%	20.70%
67	19.17%	16.62%	28.11%	22.74%
69	19.34%	17.02%	31.11%	23.70%
71	18.76%	17.02%	31.32%	21.67%
73	19.57%	18.18%	32.67%	22.52%
75	20.63%	18.00%	33.47%	25.90%
77	20.65%	18.59%	36.72%	23.24%
79	21.83%	21.04%	39.87%	24.55%
81	21.88%	22.24%	41.41%	21.98%
83	25.23%	24.78%	45.82%	26.12%
85	27.99%	28.91%	50.05%	33.29%
87	35.13%	35.07%	57.63%	42.13%
89	39.46%	39.00%	62.86%	45.91%
91	40.15%	47.59%	71.53%	45.32%
93	55.29%	61.11%	88.18%	60.11%
95	61.12%	70.13%	98.03%	66.35%
97	70.71%	83.37%	116.48%	74.01%
99	62.99%	87.55%	129.05%	74.98%

Table 12: Errors for the ROI position cases for the ^{137}Cs/^{135}Cs

Position (cm)	Case 1	Case 2	Case 3	Case 4
1	14.83%	19.40%	11.78%	14.01%
3	22.07%	23.03%	19.98%	20.86%
5	20.67%	21.47%	19.36%	20.22%
7	17.93%	17.70%	16.25%	17.25%
9	14.73%	15.25%	13.75%	14.55%
11	12.35%	13.03%	11.77%	12.14%
13	10.70%	11.53%	10.25%	11.04%
15	9.46%	10.78%	9.22%	9.69%
17	8.71%	10.02%	8.35%	8.86%
19	8.17%	9.67%	7.90%	8.31%
21	7.85%	9.54%	7.54%	8.07%
23	7.61%	9.47%	7.32%	7.93%
25	7.48%	9.55%	7.22%	7.79%
27	7.47%	9.66%	7.23%	7.76%
29	7.56%	9.85%	7.27%	7.90%
31	7.57%	9.99%	7.32%	8.03%
33	7.77%	10.15%	7.34%	8.13%
35	7.79%	10.36%	7.42%	8.16%
37	7.77%	10.52%	7.44%	8.15%
39	7.89%	10.56%	7.30%	8.39%
41	8.06%	10.76%	7.36%	8.42%
43	8.10%	10.94%	7.51%	8.54%
45	8.18%	10.92%	7.56%	8.48%
47	8.21%	11.05%	7.71%	8.48%
49	8.33%	11.13%	7.70%	8.48%
51	8.39%	11.01%	7.66%	8.33%
53	8.18%	10.99%	7.50%	8.55%
55	8.19%	10.81%	7.55%	8.41%
57	8.15%	10.87%	7.58%	8.35%
59	8.05%	10.64%	7.49%	8.16%
61	7.87%	10.58%	7.38%	8.24%
63	7.74%	10.41%	7.35%	8.20%
65	7.79%	10.33%	7.22%	8.01%
67	7.63%	10.04%	7.24%	7.98%
69	7.58%	9.92%	7.13%	7.89%
71	7.50%	9.72%	7.19%	7.88%
73	7.48%	9.57%	7.20%	7.79%
75	7.53%	9.48%	7.30%	7.83%
77	7.69%	9.50%	7.39%	7.95%
79	7.83%	9.53%	7.69%	8.15%
81	8.18%	9.85%	7.96%	8.56%
83	8.74%	10.24%	8.58%	9.15%
85	9.86%	11.15%	9.42%	9.90%
87	11.53%	12.32%	10.73%	11.06%
89	13.25%	13.86%	12.42%	12.86%
91	15.07%	15.58%	14.57%	15.42%
93	18.14%	18.80%	17.28%	18.20%
95	21.07%	21.32%	20.44%	20.74%
97	22.72%	24.06%	19.83%	22.10%
99	15.39%	20.08%	12.34%	14.55%

APPENDIX B

INDIVIDUAL ISOTOPE GROWTH COMPARISON FOR ROD POSITION CASES
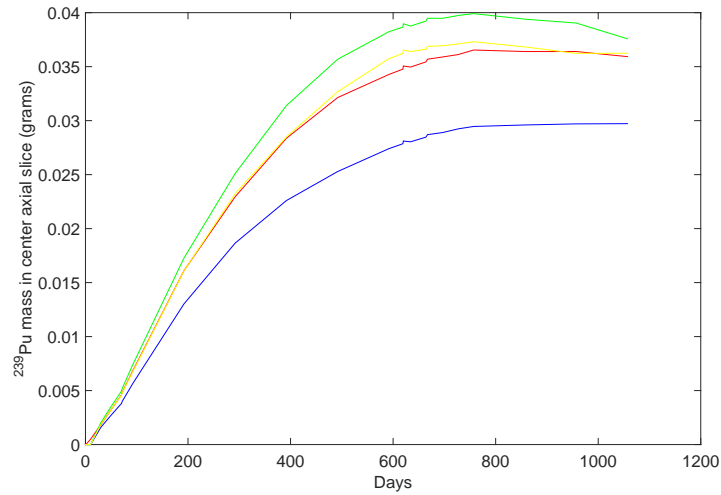

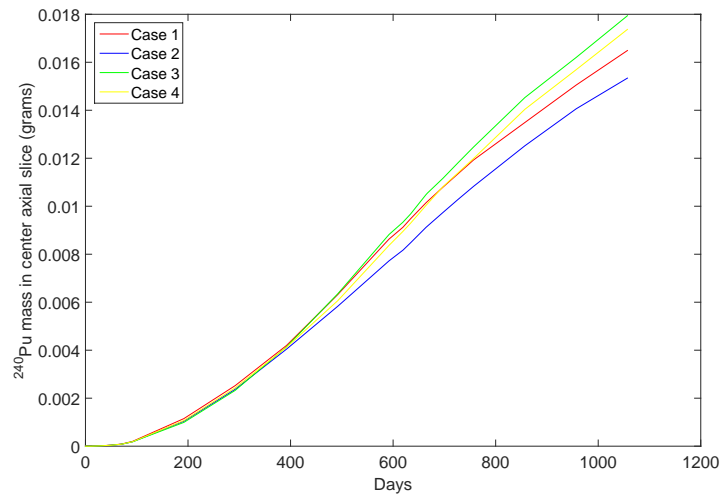Figure 36: ^{239}Pu mass in center-most axial slice versus irradiation time

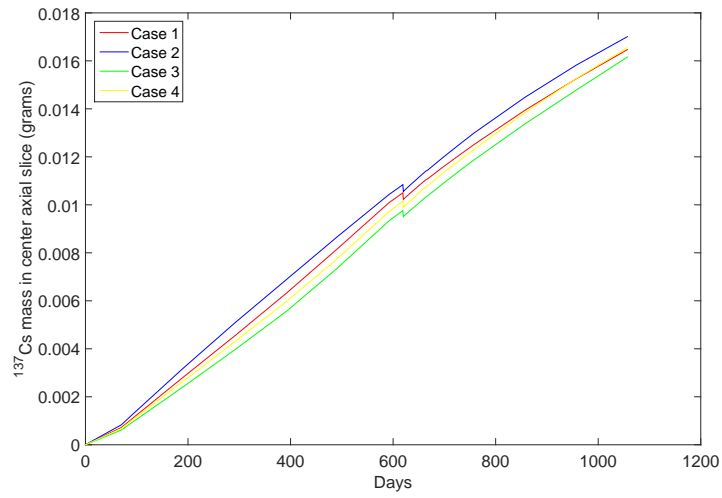Figure 37: ^{240}Pu mass in center-most axial slice versus irradiation time

Figure 38: ^{137}Cs mass in center-most axial slice versus irradiation time
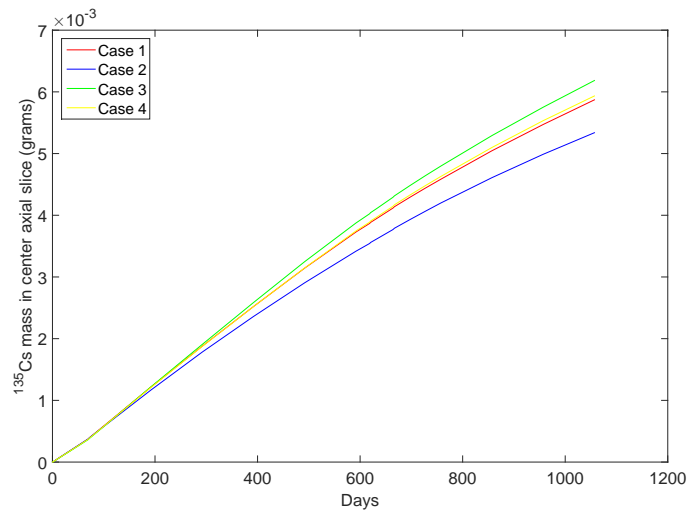

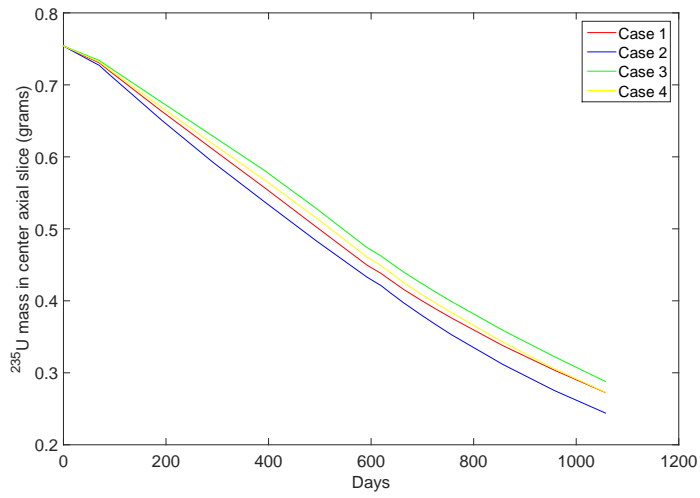Figure 39: ^{135}Cs mass in center-most axial slice versus irradiation time

62

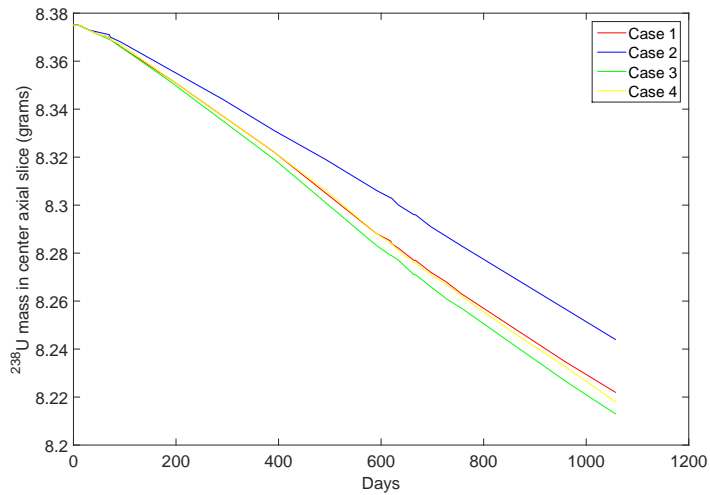Figure 40: ^{235}U mass in center-most axial slice versus irradiation time

Figure 41: ^{238}U mass in center-most axial slice versus irradiation time

63

APPENDIX C

SAMPLE MCNP INPUT

Inputs for the assembly model were rather long and would be too long to fit in this thesis. An input for the pellet model in MCNP is included below. Please email aconant3@gatech.edu if you would like access to other inputs.

```
BR3 Fuel Pin
c 08-26-2015
c === Cell Cards ===
100 1 -10.202 -1 15 -16 vol=1.015387878 imp:n=1 tmp=8.73163E-08
200 2 -6.5 -2 1 15 -16 imp:n=1 tmp=4.73308E-08
300 3 -0.79288 2 11 -12 13 -14 15 -16 imp:n=1 tmp=4.61570E-08
400 0 -11:12:-13:14:-15:16 imp:n=0
c === Surface Cards ===
1 cz 0.4020
2 cz 0.4525
*11 px -0.6750
*12 px 0.6750
*13 py -0.6750
*14 py 0.6750
*15 pz 0
*16 pz 2
c === Data Cards ===
BURN POWER=0.000425
TIME= 1 9 20 20 20 19 $ 70-day cycle, 19 day shutdown
```

2 20 100 100 100 100 100 27 $ 522 days at 82.5%, 27 days at 70% power

3 30 100 100 100 100 $ 433 days of shutdown

1 14 30 24 $ 45 days at 88%, 24 days of shutdown

3 30 30 30 100 100 100 $ 393 days at 82%

10 55 100 100 100 3287.25 7305 $ 1, 9, 20 years of cooling

PFRAC= 0.486 0.486 0.486 0.486 0.486 0.0

0.826 0.826 0.826 0.826 0.826 0.826 0.826 0.7

0 0 0 0 0 0

0.881 0.881 0.881 0

0.821 0.821 0.821 0.821 0.821 0.821 0.821

0 0 0 0 0 0 0

MAT= 1

MATVOL= 1.015387878

BOPT=1.0 -24

OMIT= -1, 90, 6014

7016, 8018, 9018,90234,91232,95240,95244,94245,97245,97246,97247,97248,

12027,13026,13028,14027,34081,35080,36081,38085,39092,39093,40089,69168,

40097,41091,41092,41096,41097,41098,41099,41100,42093,42101,43097,43098,

44097,45104,45106,45107,45108,45109,46103,46109,46111,46112,47106,47108,

47110,48107,48109,48115,49114,49116,49117,49121,49122,49123,52127,52129,

53128,53132,53133,53134,54127,56131,58137,60149,61145,61146,62145,62146,

64150,64151,64159,66157,66159,67163,67164,67166,68163,68165,69166,69167,

90231,90233

m1 92235.73c -0.0728

92238.73c -0.8086

8016.73c -0.1186

m2 40090.71c -1

65

m3 1001.71c -0.11111

8016.71c -0.88889

mt1 u/o2.17t

o2/u.17t

mt2 lwtr.15t

kcode 5000 1.5 50 750

ksrc 0 0 1

F4:N 100

F14:N 100

FM14 (1 1 -6)

(1 1 -2)

APPENDIX D

AUSPICES STATEMENTS

The material is based upon work supported under an Integrated University Program Graduate Fellowship.

REFERENCES

[1] *Directory of Nuclear Reactors*, vol. 2. International Atomic Energy Agency, 1966.

[2] *MCNP6 User's Manual*, May 2013.

[3] ADAMS, J. and DABELL., B., "Characteristics of uo2-zr fuel rods irradiated in the br3 reactor," tech. rep., Idaho National Engineering Laboratory, 1984.

[4] BRADY-RAAP, M., COLLINS, B., LYONS, J., and LIVINGSTON, J., "Fy13 summary report on the augmentation of the spent fuel composition dataset for nuclear forensics: Sfcompo/nf," tech. rep., Pacific Northwest National Laboratory, 2014.

[5] CHADWICK, M., "Endf/b-vii.1 nuclear data for science and technology: Cross sections, covariances, fission product yields and decay data," *Nuclear Data Sheets*, vol. 112, no. 12, pp. 2887–2996, 2011.

[6] CHARLIER, A., "Experimental study of the tritium invenory in the br3 and extrapolation to a p.w.r. of 900 mwe," *Commission of the European Communities: Nuclear Science and Technology*, 1982.

[7] CONLIN, J., PARSONS, D., GARDINER, S., GRAY, M., KAHLER, A., WHITE, M., and LEE, M., "Listing of available ace data tables," tech. rep., Los Alamos National Laboratory, 2014.

[8] DADOUMONT, J., MASSAUT, V., and VERMEERSCH, F., "The br3 decommissioning project: a pilot for submarine reactors," tech. rep., SCK-CEN, 1999.

[9] DELMORE, J., SNYDER, D., TRANTER, T., and MANN, N., "Cesium isotope ratios as indicators of nuclear power plant operation," *Journal of Environmental Radioactivity*, vol. 102, pp. 1008–1011, 2011.

[10] FEDCHENKO, V., "The rold of nuclear forensics in nuclear security," *Strategic Analysis*, vol. 38, no. 2, pp. 230–247, 2014.

[11] FENSIN, M., JAMES, M., HENDRICKS, J., and GOORLEY, J., "The new mcnp6 depletion capability," tech. rep., Los Alamos National Laboratory, 2012.

[12] FERRENBERG, A. and LANDAU, D., "Statistical and systematic errors in monte carlo sampling," *Journal of Statistical Physics*, 1991.

[13] GARCIA-HERRANZ, N., CABELLOS, O., SANZ, J., JUAN, J., and KUJIPER, J., "Propogation of statistical and nuclear data uncertainties in monte carlo burn-up calculations," *Annals of Nuclear Energy*, 2008.

[14] GOORLEY, J., "Initial mcnp6 release overview - mcnp6 version 1.0," tech. rep., Los Alamos National Laboratory, 2013.

[15] HILL, D., "Nuclear core arrangement," 1982.

[16] HOLMER, D., "Nuclear materials control and accountability," tech. rep., U.S. Department of Energy, 2012.

[17] HUTCHEON, I., KRISTO, M., and KNIGHT, K., "Nonproliferation nuclear forensics," tech. rep., Glenn Seaborg Institute, Lawrence Livermore National Laboratory, 2012.

[18] ILAS, G., GAULD, I., DIFILIPPO, F., and EMMETT, M., "Analysis of experimental data for high burnup pwr spent fuel isotopic validation - calvert cliffs, takahama, and three mile island reactors," tech. rep., Nuclear Regulatory Commission, 2010.

[19] JONES, A., TURNER, P., ZIMMERMAN, C., and GOULERMAS, J., "Classification of spent reactor fuel for nuclear forensics," *Journal of Analytical Chemistry*, 2014.

[20] KIM, J., HAN, S., SUH, M., JOE, K., and EOM, T., "Burnup measurement of irradiated uranium dioxide fuel by chemical methods," *Journal of the Korean Nuclear Society*, vol. 21, no. 4, 1989.

[21] KIM, J., JEON, Y., PARK, S., HA, Y., and SONG, K., "Analysis of high burnup pressurized water reactor fuel using uranium, plutonium, neodymium, and cesium isotope correlations with burnup," *Nuclear Engineering Technology*, 2015.

[22] M. WALLENIUS, TITLE = NUCLEAR FORENSICS INVESTIGATIONS WITH A FOCUS ON PLUTONIUM, J. . J. Y. . .

[23] MERTYUREK, U., "Scale 5 analysis of bwr spent nuclear fuel isotopic compositions for safety studies," tech. rep., Oak Ridge National Laboratory, 2010.

[24] MOODY, K., GRANT, P., and HUTCHEON, I., *Nuclear Forensic Analysis.* CRC Press, 2nd ed., 2014.

[25] NICHOLS, A., ALDAMA, D., and VERPELLI, M., "Handbook of nuclear data for safeguards: Database extensions, august 2008," tech. rep., International Atomic Energy Agency, 2008.

[26] NICOLAOU, G., "Discrimination of spent nuclear fuels in nuclear forensics throught isotopic fingerprinting," *Annals of Nuclear Energy*, vol. 72, pp. 130–133, 2014.

[27] OTT, L., "Mixed-oxide (mox) fuel performance benchmark," tech. rep., Oak Ridge National Laboratory, 2009.

[28] ROBEL, M., "Application of plutonium and cesium isotope ratio measurements to estimate the duration fo irradiation of spent reactor fuel," *Manuscript in preparation*, 2015.

[29] SHULTIS, J. and FAW, R., *An MCNP Primer.* Department of Mechanical and Nuclear Engineering, Kansas State Unviersity.

[30] STORRER, J., "Br3/vulcain nuclear power station construction and operational experience," tech. rep., Belgonucleaire, S.A., 1968.

[31] TAKEDA, T., HIROKAWA, N., and NODA, T., "Estimation of error propagation in monte-carlo burnup calculations," *Journal of Nuclear Science and Technology*, 199.

[32] TAYLOR, V., EVANS, R., and CORNETT, R., "Preliminary evaluation of 135cs/137cs as a forensic tool for indentifying source of radioactive contamination," *Journal of Environmental Radioactivity*, 2008.

[33] TODREAS, N. and KAZIMI, M., *Nuclear Systems I.* Taylor & Francis Group, LLC, 1990.

[34] WILSON, W., COWELL, S., ENGLAND, T., HAYES, A., and MOLLER, P., *A Manual for CINDER'90 Version 07.4 Codes and Data*, 2007.

[35] YAMAMOTO, T., KAWASHIMA, K., ANDO, Y., SAKURADA, K., HAYASHI, Y., AOKI, S., and AZEKURA, K., "Analysis of core physics experiments on fresh and irradiated br3 mox fuel in rebus program," *Journal of Nuclear Science and Technology*, 2009.